Conversion of Municipal Solid Waste to Energy

By:
Naseem Agha
Elias Azar
Kevin Bahati
Ally Hermans

Table of Contents

1. Summary

The United States lacks efficient separation of waste materials and recycling methods, resulting in an environment that generates more waste than able to maintain. Landfills contribute to pollution, carbon emissions, and other environmental hazards that are detrimental to future generations. Along with this issue, the demand for energy is projected to increase with our current growing population, therefore, repurposing waste to energy is a resourceful approach to addressing the landfill crisis.

The waste-to-energy process utilizes Boulder's municipal solid waste (MSW), generated at 205,656 kg per day, maintaining the county's goal to minimize waste while supplying valuable energy. A gasification unit and solid oxide fuel cell, coupled with a Rankine cycle, is modeled to break down MSW to syngas and capture energy, respectively. The fuel cell and Rankine cycle will produce 7.82 MW of energy, supplying enough electricity to power the process, with a remaining amount to be sold for profit to local utility companies. This process also includes a syngas cleanup unit and water gas shift unit to remove any fuel cell toxicities during the process and improve cell efficiency. Carbon dioxide is recognized as one of the major greenhouse gases that contributes to global warming. The 7,550 kg/hr of carbon dioxide produced throughout this process will be captured and stored underground using various separation units, including a packed absorber and packed stripper, thus reducing carbon dioxide emissions from the process to the atmosphere.

The total plant capital cost for our plant is $69,987,562 , and the cost of manufacturing is $36,192,437. The total revenue expected is $31,664,680 annually if the metals and glass recovered within the process will be of sellable quality, and $13,362,280 annually without revenue from both materials. Without revenue from recovered metals and glass, our plant will

not be profitable over 20 years, which is the assumed lifetime of the plant. With the anticipated revenue from both materials, the IRR is 40.7%.

2. Introduction

With the growth of the world's population and a progressive increase in living standards, the consumption of goods and energy continues to increase, provoking land-use changes and deforestation, intensified agricultural practices, and industrial reliance on fossil fuel sources. This trend has contributed to an increased generation of municipal solid waste (MSW). In 2012, global MSW generation levels were approximately 1.3 billion tonnes per year and are expected to increase to 2.2 billion tonnes per year by 2025. This forecast represents a significant increase in per capita waste generation rates, from 1.2 to 1.42 kg per person daily leading up to 2025 (Bhada-Tata et al., 2012).

Of the 633 recycling facilities in the United States, less than 10% of recycled materials enter the recycling stream while 15% of the recycled materials are burned in waste-to-energy facilities. The remainder is destined for landfills, where they accumulate and eventually find their way into the environment, thus contributing to pollution (O'Neill, 2018). Considering this pathway, and the fact that MSW generation rates will continue to increase with the current population growth, an approach to sustainably managing MSW is essential to control associated pollution. One approach to managing MSW is to convert it to energy, which will also help address the energy needs of a growing population (U.S. Department of Energy, 2019).

Incineration and anaerobic digestion represent two existing types of waste to energy (WTE) techniques in the United States, both of which require prior separation of recyclables to achieve optimal resource recovery. However, high operating costs and high levels of competition from alternative sources make the production of heat and power from MSW economically

challenging (U.S. Department of Energy, 2019). Conversely, a compelling alternative to both approaches is gasification, because it is more efficient and cleaner relative to incineration and anaerobic respiration in terms of greenhouse emissions it poses. This work details the design of a plant that converts MSW to electricity.

3. Background and Previous Work

The vast majority of the waste to energy (WTE) systems in the U.S. are located along the West Coast and the Northeast regions (U.S. Department of Energy, 2019). The city of Boulder, Colorado plans to recycle 85% of waste materials by the year 2025 rather than sending the materials to landfill (City of Boulder, 2015). The city also lacks WTE systems that can facilitate its waste reduction plan. The estimated generation of MSW from Boulder is assumed to be 205,656 kilograms per day (Funk et al., 2013). This waste will be the feedstock to the WTE process detailed in this work.

Gasification is a thermochemical conversion of carbonaceous materials into gaseous products at high temperatures with the aid of a gasification agent. The gasification agent is a gaseous compound that allows the feedstock to be converted into gas by means of various heterogeneous reactions (Yong et al., 2017). The gaseous product obtained during this process is called synthetic gas (syngas) or producer gas, and it mainly contains hydrogen, carbon monoxide, carbon dioxide, and methane. Furthermore, small amounts of inert gases, hydrocarbons, tars, and gas pollutants can be formed during the gasification process. Syngas can be utilized as a gas fuel for an engine or combusted in a conventional furnace. It can also be used as a building block for producing valuable products, such as chemicals and other forms of fuel energy (Yong et al., 2017). Gasification can be divided into two categories based on the effect of the gasification agent. If a gasification agent partially oxidizes the feed material, it refers to

direct gasification. During direct gasification, oxidation reactions supply the required energy to maintain the temperature of the process. If the gasification process takes place without the aid of a gasification agent, it refers to indirect gasification. Oxygen or air can be used as a gasifying agent in direct gasification. Air as a gasifying agent reduces the heating value of syngas due to the presence of nitrogen. Pure oxygen as a gasifying agent overcomes reduction. However, the cost of producing pure oxygen accounts for more than 20% of the total cost of electricity production in a WTE plant (Yong et al., 2017). Steam is usually used for indirect gasification as it is easily available. Moreover, it increases the hydrogen content in the syngas gas formed . The gasification process generally consists of four main physical and chemical reaction stages: drying, pyrolysis, gasification, and combustion. The location of these stages within the gasifier determines whether the gasifier is configured as a downdraft gasifier or an updraft gasifier. Both configurations have advantages and disadvantages that suit them for varying applications.

Before syngas can be fed as fuel to a solid oxide fuel cell, it must be cleaned of any contaminants and its composition must include a sufficient amount of hydrogen for better fuel cell efficiency. Hydrogen sulfide is one of the harmful chemicals in syngas produced from gasification that have to be cleaned out because it degrades the fuel cell (Marcantonio, 2002). To remove this contaminant, the syngas stream can be fed to a reactor packed with solid zinc oxide particles, which reacts with the hydrogen sulfide from the stream to form solid zinc sulfide and water vapor. Previous work on desulfurization utilizes this technique with metal oxide sorbent particles, typically with either zinc oxide or iron oxide particles. Zinc oxide is used more as a sorbent relative to iron oxide because it is thermodynamically more favorable in terms of efficiently desulfurizing the gas stream (Gupta, 2007). To increase the hydrogen content of the

syngas, the carbon monoxide can undergo a water-gas shift reaction to form hydrogen and carbon dioxide.

The renewable sector currently looks to fuel cells in terms of energy efficiency, one such system being the solid oxide fuel cell (SOFC). This type of fuel cell has seen success for its versatility: acceptance of a wide range of hydrocarbon fuels due to internal reforming, state of the art efficiency, and minimal greenhouse gas and pollutant emissions. Whereas traditional burners require conversion of chemical potential to thermal energy, then to electricity through mechanical work, SOFCs provide a solution in going straight from chemical potential to electricity. This simplification means less heat losses throughout, allowing the fuel cell to reach up to 80% efficiency (EG&G, 2004). This efficiency is achieved through the electrolytic reaction of oxygen with hydrogen and carbon monoxide. To distinguish this reaction over combustion, the oxygen source (cathode) is separated from the fuel source (anode) by an oxygen ion permeable interface in the form of a yttrium stabilized zirconia (YSZ) electrolyte. Air flows through the cathode, where oxygen reacts on the surface to form its ionic counterpart. These ions flow to the anode side of the electrolyte, where they interact on the surface with feedstock on the surface, producing water, carbon dioxide, heat, and a source of electrons. It is worthwhile to note that the anode material, a cermet composed of YSZ and nickel, is sensitive to hydrogen chloride and sulfide poisoning (EG&G, 2004). SOFCs operate with unavoidable heat waste. Therefore, they are often used in conjunction with heat loss recovery systems such as the Rankine Cycle. The Rankine Cycle is an idealized limit to the steam engine, where an external heat source is converted into mechanical work through four stages: isentropic compression, isobaric heating, isentropic expansion, and isobaric cooling. The Rankine Cycle's performance is limited by its Carnot Efficiency.

Carbon dioxide produced in a waste-to-energy process can be trapped, isolated, and transported to underground storage locations, thus making the overall process more environmentally friendly (Leung et al., 2014). This process can occur in two main stages: one stage utilizing an absorption column to absorb the CO_2 gas using a solvent , and the other stripping column the CO_2 from the hot solvent from the absorber. The reduced captured CO_2 coming off the stripper can be separated from water using a flash vessel, and transported off to an underground storage site onsite. Monoethanolamine (MEA) is a commonly used solvent in the absorber because it is cheaper relative to other solvents, biodegradable, and readily reacts with CO_2 (Luis, 2016).

4. Final Design

4.1 *Process Overview*

As shown in Figure 4.1-1, our process is made up of six main stages: feedstock preparation, gasification, syngas cleanup, water-gas shift reaction, solid oxide fuel cell, and carbon capture. The feed to the process is 9,858 $\frac{kg}{hr}$ of MSW from the city of Boulder, Colorado. The primary product is 7.29 MW of electricity produced by the SOFC.

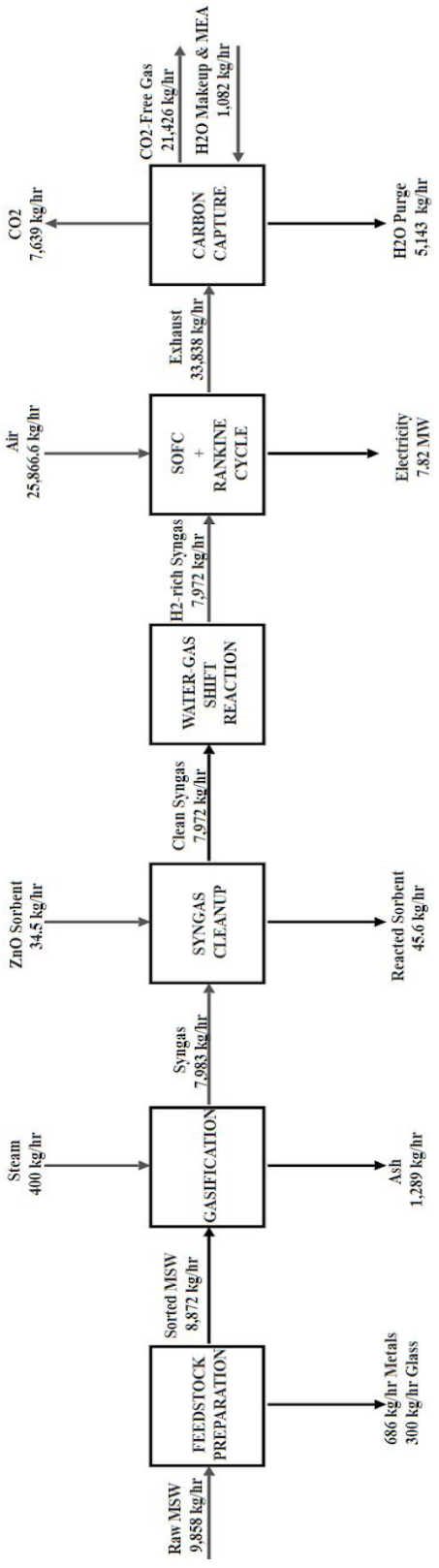

Figure 4.1-1: BFD of overall waste-to-energy process

4.2 Feedstock Characterization

The raw MSW feedstock to the process was assumed to contain 3% glass and 7% metals by mass based on typical metal and glass composition in MSW. The moisture content in the wet MSW feedstock to the gasification stage was assumed to be 37.45% by mass, which is the average moisture content from 20 different MSW samples found by Taufiq. Furthermore, the content of ash in the raw feedstock was assumed to be 14.5% by mass based on the work of Golam that states that the content of ash in MSW is typically 14-17% by mass. Considering this, 9,858 kg/hr of raw MSW was fed to the overall process, and 8,872 kg/hr of wet MSW was fed to the gasification stage of the process.

Table 4.2-1: Composition of feedstock to the WTE process

Component	Mass (kg/hr)
H	318
N	207
C	2,060
O	2,148
S	10
Water	2,840
Ash	1,289
Metals	686
Glass	300
Total raw feedstock	9,858

4.3 Feedstock Preparation

As shown in Figure 4.3-1, the feedstock preparation part of the process involves the separation of metals and glass from raw MSW, and also the shredding of the resulting stream that is then fed to the gasification system. First, the raw MSW feedstock is moved from a storage pit to a section of the process where metals and glass are removed. The storage pit was designed to hold a capacity of 6,648 m^3 of raw MSW, which is equivalent to MSW generated by the city of Boulder over the course of two weeks. The storage pit costs $503,000. Its cost was approximated as the cost of storage tanks that can handle an equivalent capacity of MSW. A screw conveyor was designed to move raw MSW from the storage pit. The screw conveyor is designed according to the specifications in Table 4.3-1, costs $24,000, and consumes 4.5 kW of electric power. The SOFC will provide the electric power needed (see section 4.7).

Table 4.3-1: Design specifications of screw conveyor moving raw MSW from storage.

Design Criterion	Units	Value
Diameter	cm	50.8
Screw Pitch	cm	50.8
Auger Speed	RPM	36
Conveyor Length	m	6.1
Power	kW	4.6
Bare Module Cost	USD	$9,143

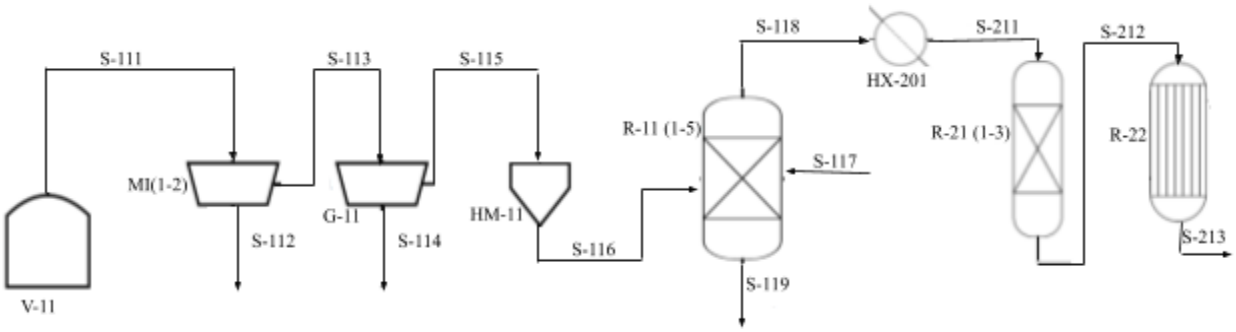

Figure 4.3-1: PFD of the upstream process including combined feedstock preparation, gasification stages, syngas cleanup reactor, and water gas shift reactor.

Ferrous metals are first separated out from raw MSW, followed by non-ferrous metals. A 3kW CT6018 magnetic drum separator from Xi'an Desen Mining Machinery Equipment Co., Ltd was chosen for separating out ferrous metals and costs $10,000. A 15kW QJWDL Eddy current separator from CHANMAG was chosen for separating out non-ferrous metals and costs $19,000. The electric power needed by both the Eddy current separator and the magnetic drum will be provided by the SOFC (see section 4.7). A screw conveyor was designed to move MSW free of ferrous metals from the magnetic drum to the Eddy current separator. The screw conveyor was designed according to the specifications in Table 4.3-2**,** and costs $6,930. The 0.34 kW of electric power needed by this screw conveyor will be provided by the SOFC (see section 4.7). The magnetic drum combined with the Eddy current separator are expected to recover 98% of metals, yielding a minimum of 672 kg/hr of metals (both ferrous and non-ferrous).

Table 4.3-2: Design specifications of screw conveyor moving MSW from magnetic drum to Eddy current separator.

Design Criterion	Units	Value
Diameter	cm	50.8
Screw Pitch	cm	50.8
Auger Speed	RPM	36
Conveyor Length	m	3.05
Power	kW	0.46
Bare Module Cost	USD	$6,930

After the removal of metals, the resulting MSW is fed to a glass sorting machine that removes a minimum of 98% of glass in the feed. Autosort Color, manufactured by Tomra, was chosen for this purpose. Based on the costs of similar equipment meant for different purposes on Alibaba, the equipment is expected to cost $40,000 maximum and consume 10 kW of electricity at maximum. A screw conveyor was designed to move MSW from the Eddy current separator to the AutoSort Color. The design specifications for this screw conveyor are shown in Table 4.3-3. A minimum of 294 kg/hr of glass is expected to be recovered.

Table 4.3-3: Design specifications of screw conveyor moving MSW from Eddy current separator to glass sorting machine.

Design Criterion	Unit	Value
Diameter	cm	50.8
Screw Pitch	cm	50.8
Auger Speed	RPM	33
Conveyor Length	m	3.05
Power	kW	0.42
Bare Module Cost	USD	$6,930

The fully sorted MSW is then moved to a combined-shaft shredder (HM-11 in Figure 4.3-1) manufactured by Shouyu Machinery. This equipment pelletizes the sorted MSW into 1 cm particles that can readily react in the gasifier. The equipment costs $168,000 and requires a combined 330 kW of electric power, which will also be provided by the SOFC (see section 4.7). A screw conveyor was designed to move the MSW to this equipment. The specifications of the screw conveyor are shown in Table 4.3-4. The shredded MSW, stream S-117, is then fed to the gasifier.

Table 4.3-4: Design specifications of screw conveyor moving MSW from glass sorting to glass shredding.

Design Criterion	Units	Value
Diameter	cm	50.8
Screw Pitch	cm	50.8
Auger Speed	RPM	31
Conveyor Length	m	6.1
Power	kW	0.81
Bare Module Cost	USD	$9,140

Table 4.3-5: Material recovery results from feedstock preparation, assuming perfect recovery.

Material	Units	Mass	Stream
Metals	kg/hr	686	S-112
Glass	kg/hr	300	S-114
Sorted, pelletized MSW	kg/hr	8,872	S-116
Totals	kg/hr	9,858	

4.4 Gasifier

The PFD of the gasification system is shown in Figure 4.3-1. Our gasifier system of five gasifiers was designed to process 8,872 kg/hr of sorted and pelletized MSW (stream S-116 in PFD), with each processing 1,774 kg/hr. Steam (stream S-117 in the PFD) was fed to each of the gasifiers as a gasifying agent. Our design can handle a 25% increase in MSW generated in the city of Boulder. The products from our gasification system are syngas (stream S-118) and ash (stream S-119). Based on a hearth load of 150 kg/m^{2}h, we calculated the required diameter to be 4 meters and the length to be 12 meters. The full design specifications of each of our five gasifiers are shown in Table 4.4-1. The cost of each gasifier was determined using CAPCOST.

Table 4.4-1: Design specifications for each of the five gasifiers.

Variable	Units	Value
Diameter	m	4
Height	m	12
Load Per Gasifier	kg/hr	1,774
Heat Duty	MW	2.2
Cross-Sectional Area of Grate	m^2	12.6
Bare Module Cost	USD	$1,613,000

Considering that we have five gasifiers, our gasification system costs $8,065,000 and has a combined heat duty of 10.8 MW.

Table 4.4-2: Results from gasification system.

Component	Unit	S-116	S-117	S-118	S-119
H_2	kg/hr	0	0	149	0
NH_3	kg/hr	0	0	0.45	0
CH_4	kg/hr	0	0	424	0
N_2	kg/hr	0	0	217	0
CO	kg/hr	0	0	1,490	0
H_2S	kg/hr	0	0	11.1	0
CO_2	kg/hr	0	0	1,590	0
H_2O	kg/hr	0	400	3,390	0
Tars	kg/hr	0		711	
Ash	kg/hr	0	0	0	1,289
MSW	kg/hr	8,872	0	0	0
Subtotals	kg/hr	8,872	400	7,983	1,289
Total	kg/hr	Inlet	9,272	Outlet	9,272
Temperature	°C	25	700	700	700
Pressure	bar	3	5	5	5

A system of screw conveyors was designed to insert the sorted pelletized MSW into the gasifiers. Each gasifier has one such conveyor, so a total of five screw conveyors are needed. The design specifications of each of these conveyors are shown in Table 4.4-3. The conveyors cost a combined $43,100 and require a combined electric power of 2.6 kW, which will be provided by the SOFC.

Table 4.4-3: Showing design specifications for each of the screw conveyors inserting MSW into each of the gasifiers.

Design Criterion	Unit	Value
Diameter	cm	35.6
Screw Pitch	cm	35.6
Auger Speed	RPM	59.2
Conveyor Length	m	7.6
Power	kW	0.51
Bare Module Cost	USD	$8,620

Another system of five screw conveyors was designed to withdraw ash (stream S-119) from the bottom of each of the gasifiers. The design specifications of each of these screw conveyors are shown in Table 4.4-4. The conveyors require a combined electric power of 0.62kW and cost $31,600.

Table 4.4-4: Design specifications of screw conveyors withdrawing tars from gasifiers

Design Criterion	Units	Value
Diameter	cm	22.9
Screw Pitch	cm	22.9
Auger Speed	RPM	109
Conveyor Length	m	7.6
Power	kW	0.11
Bare Module Cost	USD	$6,320

4.5 Syngas Cleanup

As shown in Figure 4.3-1, the syngas stream from gasification (S-118) is cooled, then fed to the syngas cleanup reactor (R-21). The heat exchanger (HX-201) cools the gas from 700°C to 400°C with water flowing counter-currently in the shell at 184°C and at 2,260 kg/h. The area of the heat exchanger is 121 m^2. A pump (P-201) was designed to pressurize the hot water for this heat exchanger and for the WGS reactor (R-22). The heat exchanger converts all of the hot water to steam at 184°C and at 2,260 kg/h, which will be utilized in the reboiler of the carbon capture system (Section 4.9). Next, the cooled syngas stream (S-211) is fed to a reactor (R-21 in Figure 4.3-1) that removed the hydrogen sulfide. This system uses a simulated moving bed including three packed reactors, shown by Figure 4.5-1. Each reactor is filled with a zinc oxide solid sorbent. Two of these reactors are utilized at a time, while the third will be cleaned and filled with fresh sorbent. The reactors are designed to hold enough sorbent particles for a year. Therefore, sorbent particles will only need to be changed and rotated once a year.

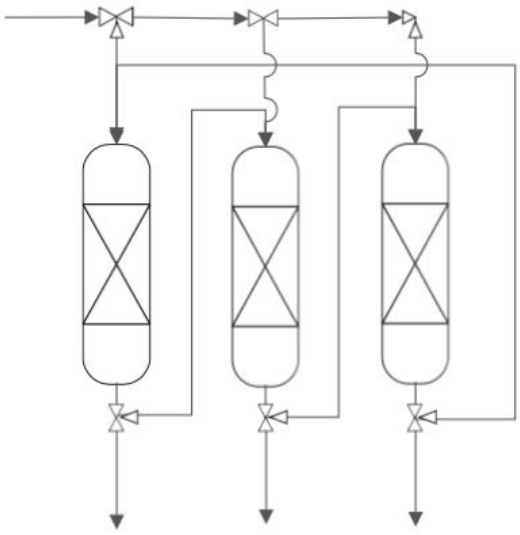

Figure 4.5-1: PFD of simulated moving bed

Each reactor is made of stainless steel and is 3 meters in diameter and 5.69 meters in length. Cylindrical zinc oxide sorbent particles are 6 mm in diameter. Sorbent particles are utilized at 275,400 kg annually, costing $1.5 million annually according to Bulk Apothecary. The bare module cost of each reactor priced using CAPCOST software is $610,000. The balanced stream compositions around the reactor are shown in Table 4.5-1, which appears unbalanced due to the difference between mass removed from the syngas and mass exchanged with the solid sorbents, totaling 5.2 kg/hr remaining in the packed bed.

Table 4.5-1: Syngas cleanup stream compositions.

Component	Units	S-211	S-212
H_2	kg/hr	149	149
NH_3	kg/hr	0.45	0.45
CH_4	kg/hr	424	424
N_2	kg/hr	217	217
CO	kg/hr	1,490	1,490
H_2S	kg/hr	11.09	0.01
CO_2	kg/hr	1,590	1,590
H_2O	kg/hr	3,390	3,400
Tars	kg/hr	711	711
Subtotals	kg/hr	7,983	7,983
Temperature	C	400	400
Pressure	bar	4.00	3.98

4.6 Water-Gas Shift

As shown in Figure 4.3-1, the product stream from syngas cleanup (stream S-212) undergoes a water-gas shift reaction in a plug flow reactor. The reactor was constructed to be similar to a shell and tube heat exchanger. The reactor contains 160 stainless tubes, each 10 cm in diameter and 1.7 m in length. The reactor was designed to achieve 87.8% conversion while operating with an iron-chromium-copper HTS catalyst. The bare module cost of the reactor calculated in CAPCOST software is $261,000. The composition of the inlet and outlet streams to the reactor are shown in Table 4.6-1.

Table 4.6-1: Water gas shift reaction stream results

Component	Units	S-212	S-213
H_2	kg/hr	149	242
NH_3	kg/hr	0.45	0.45
CH_4	kg/hr	424	424
N_2	kg/hr	217	217
CO	kg/hr	1,490	202
H_2S	kg/hr	0.01	0.01
CO_2	kg/hr	1,590	3,620
H_2O	kg/hr	3,400	2,570
Tars	kg/hr	711	711
Totals	kg/hr	7,983	7,983
Temperature	C	400	400
Pressure	bar	3.50	3.47

The reaction occurs at a constant temperature of 400°C. Due to pressure losses in piping and pressure drop in the reactor, the feed stream enters at a pressure of 3.5 bar and exits at 3.46 bar. The reaction is exothermic and generates 0.49 MW of heat. This heat is removed by boiling water where it's pumped to the shell of the reactor at 184°C and 2200 kg/hr. The boiling water leaves the reactor as steam at 184°C and 2200 kg/hr, which is utilized in the reboiler of the stripper in the carbon capture section.

4.7 Solid Oxide Fuel Cell

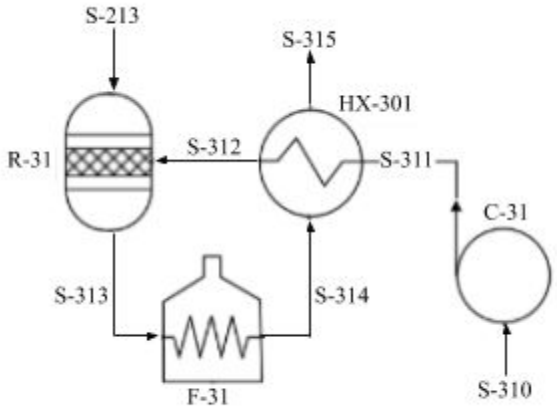

Figure 4.7-1: Solid Oxide Fuel Cell

An overview of the SOFC system is provided in Figure 4.7-1. The syngas leaving the cleanup unit is directed into the anode of the SOFC (labeled R-31 in Figure 4.7-1) and brought up to temperature from the bountiful heat losses within the system. Ambient air (stream S-310) is compressed (C-31) and fed to the cathode slightly over stoichiometry with the electrolytic reactions and combustibles downstream. Before entering the cathode, the air enters a heat exchanger (HX-301) intersected with the furnace's exhaust (stream S-314), bringing the stream up to the cell's operating temperature. The fuel cell's operating conditions are reported in Table 4.7-1 and assume a utilization factor of 85% as per literature at similar conditions. The voltage was computed using a reference voltage curve in the DoE Fuel Cell Handbook and empirical correlations that adjust for changes in temperature, pressure, and syngas and air compositions. The exhaust from the system, composed of residual syngas and vaporized tars, is fed to the furnace (R-32), where all remaining combustibles are oxidized. Since the tars are modeled as naphthalene to reflect their compositions and thermodynamic properties, they are also combusted.

The furnace is assumed adiabatic to account for minimal heat losses, where heats of combustion contribute solely to the outlet temperature. A summary of the stream compositions and operating conditions are shown in Table 4.7-1. Properties of the SOFC alongside its operating conditions are shown in Table 4.7-2.

Table 4.7-1: Fuel cell stream results

Comp.	Units	S-213	S-310	S-311	S-312	S-313	S-314	S-315
H_2	kg/hr	241.7	0	0	0	31.3	0	0
NH_3	kg/hr	0.45	0	0	0	0.45	0.45	0.45
CH_4	kg/hr	423.6	0	0	0	~ 0	0	0
N_2	kg/hr	217	22,100	22,100	22,100	22,300	22,300	22,311
O_2	kg/hr	0	6,720	6,720	6,720	3,560	865	865
CO	kg/hr	202.1	0	0	0	543	0	0
H_2S	kg/hr	~ 0	~ 0	~ 0	~ 0	~ 0	~ 0	~ 0
CO_2	kg/hr	3623.1	0	0	0	4,250	7,550	7,550
H_2O	kg/hr	2569	0	0	0	5,400	6,080	6,080
Tars	kg/hr	711.6	0	0	0	711.6	0	0
Total	kg/hr	7978	28,820	28,820	28,280	36,798	36,798	36,798
Temp.	C	400	25	169	1000	1000	1668	1189
Press.	bar	3.5	1	4	-	3.5	3	2.2

Table 4.7-2: Fuel cell stack properties

Voltage (V)	0.687	Heat Loss	5%	# of Stacks	60
T (C)	1000	Cell Area (cm^2)	834	Power (MW)	7.29
P (bar)	3	Current (A)	$10.6 \cdot 10^6$	Efficiency	60%

4.8 Rankine Cycle

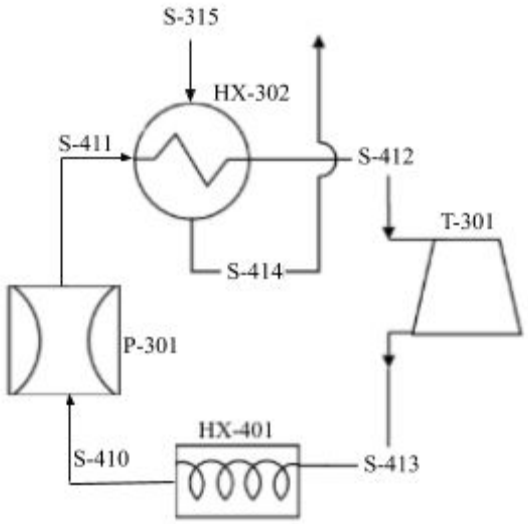

Figure 4.8-1: Rankine Cycle

Traditional gasification is endothermic, demanding a source of heat to maintain operation. This heat source was originally designated as the furnace's outlet, yet with an exothermic gasifier, a new means of heat capture was demanded: a Rankine Cycle as depicted in Figure 4.8-1b. Its circulation fluid was chosen as water due to its low flow demand, its high heat of vaporization, and its availability. The choice of a steam saturation temperature was crucial to optimizing the cycle, and it was chosen to account for the Carnot Efficiency. A pump was designed to bring room temperature water up to the saturation pressure of steam that corresponds to the high-end temperature. This pressure was determined from steam tables supplied by Felder and Rousseau. Once pressurized by the diaphragm pump (P-31), the water stream (S-411) exchanges heat with the furnace's exhaust stream (S-315) in the heat exchanger (HX-302). The flow rate of the circulating water was set to match the saturation temperature and saturation pressure, so as not to superheat the water vapor exiting the exchanger. This saturated vapor

enters an isothermal turbine (T-31) where shaft work is performed in exchange for steam decompression and cooling.

Further cooling and condensation of the steam is possible by heat transfer with ambient air over a large surface area of piping, represented as block HX-401, though this block does not model a conventional heat exchanger. Water is then recirculated through the cycle. The streams' operating conditions are summarized in Table 4.8-1, assuming negligible pressure drop through the condensation phase. The power outputs of each component are detailed in *section 4.10*.

Table 4.8-1: Rankine Cycle Stream Properties

	Units	S-315	S-414	S-410	S-411	S-412	S-413
Temp.	C	1189	390	25	28	367	102
Press.	Bar	2.2	2	1	200	200	1
Quality	Fraction	1	1	0	0	1	0.66
Flow Rate	kg/hr	37,000	37,000	15,000	15,000	15,000	15,000

4.9 Carbon Capture

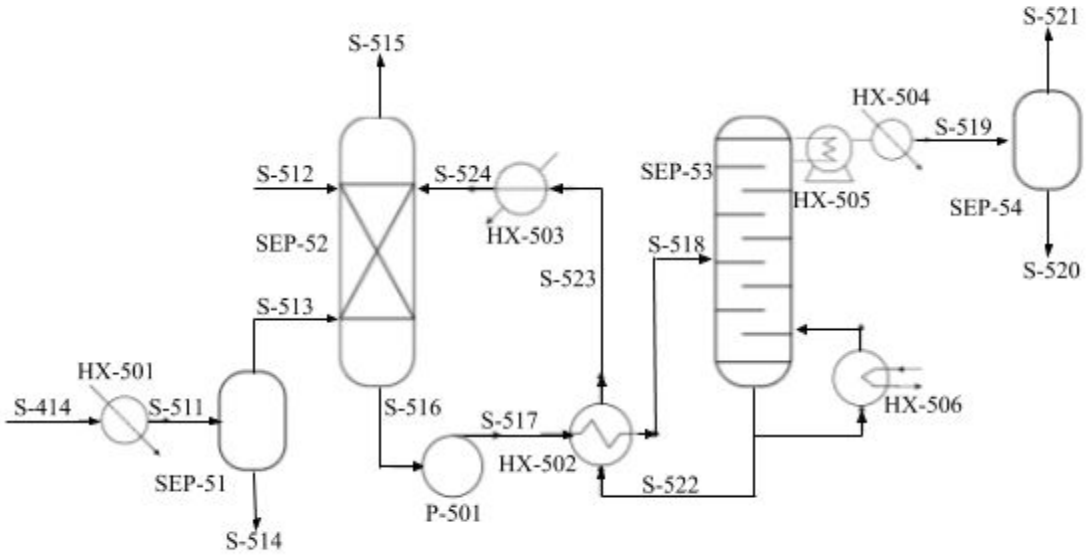

Figure 4.9-1: PFD of carbon capture system

The exhaust from the SOFC (S-414) is sent to a carbon capture and storage system that captures and stores CO_2, reducing the amount of greenhouse gases emitted to the atmosphere. As shown in Figure 4.9-1, the gas (S-414) initially enters a heat exchanger (HX-501), where it is cooled from 390°C to 50°C. This heat exchanger uses cooling water as its fluid, flowing in at 636,300 kg/hr and 25°C through the shell counter-currently, and has a heat exchanger area of 1980.06 m^2. A single heat exchanger cannot be this large, therefore, it was designed to have two shells, each with a heat transfer area of 990.03 m^2. The gas exiting the heat exchanger (S-511) enters a separating vessel (SEP-51), in which excess water is removed before absorption. All separators in this system are made of stainless steel and designed according to specifications in Table 4.9-1.

Table 4.9-1: Design dimensions for separators in the carbon capture process

Separator	Diameter (m)	Height (m)
SEP-51	2.5	2.5
SEP-52	2	9
SEP-53	1	7.9
SEP-54	0.8	0.8

The dry stream (S-514) then enters the bottom (on stage 3) of the packed absorbing column (SEP-52), in which 99.9% by mass of the carbon dioxide is absorbed by the solvent stream, and the remaining gas is vented to the atmosphere (S-515). A 30% by mass monoethanolamine (MEA) solvent makes up the inlet streams: the makeup solvent stream (S-512) and the recycled MEA solvent stream (S-524). These solvent streams enter at the top (on stage 1) of the absorption column. The rich CO_2 solvent (S-516) exits at the bottom. The dimensions of the reactor are shown in Table 4.9-1 and the design specifications are shown in Table 4.9-2.

Table 4.9-2: Design operation specifications for absorbing column (SEP-52) and stripping column (SEP-53). The packing material for both columns are made of stainless steel.

Unit	Operating Pressure (bar)	Solvent Inlet Temperature (C)	Number of Stages	Pressure Drop (bar)	Head Loss (m)	Height of Packing (m)	Packing Material
SEP-52	1.3	40	3	0.08	0.90	9	Pall Rings
SEP-53	3	125	10	0.39	4.44	4.88	Sieve Trays

Immediately after exiting the absorption column, the carbon dioxide-rich solvent (S-516) enters a centrifugal pump (P-501), raising its pressure from 1.3 bar to 5 bar, then is sent across a heat exchanger (HX-502) that raises its temperature from 71°C to 125°C. The heat exchanger utilizes the heat from the stream coming off of the bottoms of the stripper (S-522) and has a heat exchange area of 689 m^2. The prepared solvent (S-518) then enters the packed stripping column (SEP-53) at the top of the column (stage 2), which operates at 70% tray efficiency.

The MEA-rich stream coming off of the bottom of the stripper (S-522) passes through two heat exchangers before being recycled back to the absorber. First, it goes through the cross heat exchanger (HX-502) that is also used prior to stripping. This reduces the temperature from 137°C to 82°C by transferring its heat to the stream that is heated prior to entering the stripping column (S-517). Then, the gas is further cooled to 40°C with a heat exchanger that uses 25°C water flowing in through the shell counter-currently and leaving at 35°C. This shell has a heat exchanger area of 206 m^2.

The CO_2-rich stream leaving the top of the stripper enters a condenser (HX-505) and heat exchanger (HX-504) to condense the vapor and lower its temperature before entering the flash vessel (SEP-54) that separates CO_2 from H_2O. The condenser (HX-505) reduces the temperature from 125°C to 86°C with 25°C water entering co-currently in the shell and leaving at 35°C. This heat exchanger has a heat transfer area of 42.8 m^2. Immediately after, the gas enters a heat exchanger (HX-504) which uses 25°C water that flows counter-currently in the shell and leaves at 35°C, to cool the stream from 86°C to 40°C. This heat exchanger has a heat exchanger area of 559.29 m^2. The dry CO_2 stream (S-521) is the final product that we will pay for to be stored. The outlet water streams (S-514 and S-520) in this process are heavily contaminated, therefore they will be paid for as wastewater streams.

Table 4.9-2: Carbon capture stream results around the absorbing column

Comp.	Units	S-414	S-511	S-512	S-513	S-514	S-515	S-516	S-524
NH_3	kg/hr	0.45	0.45	0	0.37	0.08	0.26	0.18	0.06
N_2	kg/hr	22,311	22,300	0	22,300	0.10	22,311	0.48	0
O2	kg/hr	865	865	0	865	0.01	865	0.03	0
CO_2	kg/hr	7,550	7,550	0	7,550	1.33	10.3	3.94	0.01
H_2O	kg/hr	6,080.4	6,080	1,041	1,200	4,880	1,440	78,100	77,500
MEA	kg/hr	0	0	6.11	0	0	7.03	55,700	48,000
Temp.	C	390	50	40	50	50	51.9	70.7	40
Press.	bar	2	2	2	2	2	1.3	1.438	2

Table 4.9-3: Carbon capture stream results around the stripping column

Comp.	Units	S-517	S-518	S-519	S-520	S-521	S-522	S-523
NH_3	kg/hr	0.18	0.18	0.11	0.03	0.08	0.06	0.06
N_2	kg/hr	0.48	0.48	0.48	~0	0.48	~ 0	0
O2	kg/hr	0.03	0.03	0.03	~0	0.03	~ 0	0
CO_2	kg/hr	3.97	546	7,530	1.87	7,530	4.09	0.14
H_2O	kg/hr	78,100	78,100	800	695	105	77,500	77,500
MEA	kg/hr	55,700	55,200	0.01	0.02	~0	48,000	48,000
Temp.	C	71	125	86	45	45	137	82
Press.	bar	5	5	3	3	3	3	3

4.10 Equipment Summary

Table 4.10-1 and 4.10-3 show an equipment summary including the name and the type of the equipment, the costing metric, and the bare module cost that was estimated using CAPCOST.

Table 4.10-1: Process Equipment summary

Name	Equipment	Unit	Costing Metric	Bare Module Cost ($)
F-31	Furnace/Burner	m^3	102.5	85,900
R-11(1-5)	Gasifiers	m^3	754	8,065,000
R-21(1-3)	H_2S Reactors	m^3	241	1,830,000
R-22	WGS Reactor	m^3	85.5	216,000
R-31	SOFC	Stacks	60	17,380,000
SEP-51	Flash Drum	m^3	0.0132	154,000
SEP-52	Absorbing Column	m^3	28.27	411,000
SEP-53	Stripping Column	m^3	6.189	143,000
SEP-54	Flash Drum	m^3	0.00143	28,200
T-31	Axial Turbine	MW	2.193	3,590,000
Total				31,903,100

Table 4.10-2 shows the design summary of the heat exchangers including the condenser (HX-505) and the reboiler (HX-506) of the stripper for the carbon capture process. The heat transfer coefficient, U, for each heat exchanger was found using Peters, Timmerhaus, and West (2006) heuristics for heat exchangers. Heat exchangers were priced using CAPCOST, with stainless steel material of construction and a heat exchanger type of S/T fixed shells.

Table 4.10-2: Summary of the heat exchangers needed for the process.

Exchanger	Hot T In (℃)	Hot T Out (℃)	Cold T In (℃)	Cold T Out (℃)	Q (MW)	U (W/m^2K)	Area (m^2)
HX-201	700	400	184	184	-1.26	30	121.46
HX-301	1726	1274	169	1000	6.48	30	292.50
HX-302	1274	390	25	364	11.5	30	1,213.63
HX-501	390	50	35	25	-7.39	30	1980.06
HX-502	82	137	71	125	0	285	2067.66
HX-503	82	40	35	25	-4.90	850	206.33
HX-504	86	40	35	25	-0.56	30	559.29
HX-505	125	86	25	35	-2.65	850	42.82
HX-506	184	184	125	137	8.33	1100	143.46

Table 4.10-3: Ancillary equipment summary

Name	Equipment	Unit	Capacity	Bare Module Cost ($)
C-31	Cent. Compressor	kW	1,859	3,580,000
G-11	AutoSort Color	kg/hr	9,000	40,000
HM-11	Shredder	kg/hr	9000	168,000
HX-201	Heat Exchanger	m^2	121.46	234,000
HX-301	Heat Exchanger	m^2	292.5	345,000
HX-302	Heat Exchanger	m^2	1,213.63	702,000
HX-501	Heat Exchanger	m^2	1980.06	916,000
HX-502	Heat Exchanger	m^2	2067.66	920,000
HX-503	Heat Exchanger	m^2	206.33	292,000
HX-504	Heat Exchanger	m^2	559.29	492,000
HX-505	Condenser	m^2	42.82	170,000
HX-506	Reboiler	m^2	143.46	250,000
P-201	Centrifugal Pump	kW	0.140	19,300
P-301	Diaphragm Pump	kW	178	585,000
P-501	Centrifugal Pump	kW	19.50	38,600
V-11	Tank	m^3	6,648	503,000
	Screw conveyors	m	36	241,410
			Total	9,496,310

5. Discussion

5.1 Feedstock Characterization

The feed to the designed WTE process is the 236,592 kilograms of MSW generated in the city of Boulder, Colorado daily. Assuming 8000 hours of operation annually, our WTE plant will handle 78,872,000 kilograms of MSW annually.

The moisture content of MSW can vary from season to season. For the purpose of our simulation, we assumed a fixed moisture content of 37.45 % in wet MSW. We based the water content on the fluctuations of MSW moisture content obtained from a characterization of five different MSW samples in Dhaka, Bangladesh over four months, each in a specific season (Golam, 2016). Raw MSW typically contains ash. We considered ash to be 14.5% by mass of the raw feedstock because according to Golam, the composition of ash is typically 14-17% by mass of MSW. Of the total dry MSW mass flow to the process, 15% was assumed to be tars formed during gasification. This was based on a generation of tars that is typical of updraft gasifiers. Tars were modeled as naphthalene per the work of Lopamudra et al..

5.2 Feedstock Preparation

Feedstock preparation serves to remove metals and glass. When left in the feed to the gasifier, metals and glass can reduce the heating value of the MSW and cause constant operational problems and plant shutdowns that make WTE plants costly and unreliable (Klein, 2002). On top of this, feedstock preparation involves pelletization of MSW to create MSW with a surface area conducive for gasification reactions. Feedstock preparation can also involve drying of raw MSW to remove moisture because it reduces the efficiency of gasifying reactions and increases the energy needed for combustion. However, our feedstock was not dried before being fed to the gasifier because its water content can be tolerated by the updraft gasifiers that

have been used in our process (see section 5.3). Furthermore, external drying poses more operational costs relative to the drying that occurs within the gasifier. For raw MSW to undergo preparation, it has to be delivered from on-site storage to feedstock preparation and has to be transported within the entire process of feedstock preparation. A system of screw conveyors has been chosen for this purpose. On-site storage has been designed to hold MSW generated in Boulder over 14 days because trucks will deliver raw MSW weekly. The extra 7 days capacity accounts for possible changes in delivery periods, and is also conducive for continuous operation of the plant.

The magnetic drum separator has a 180° magnet segment, around which a stainless steel drum rotates. The magnet attracts magnetic metals that are in the raw MSW feedstock. The drum carries the attached magnetic materials with it to the bottom of the drum. There, the particles drop off and can be collected and carried away. The MSW without magnetic metals proceeds to the Eddy current separator via a screw conveyor. The Eddy current separator has a belt conveyor that has its drive located at the return end and a high-speed magnetic rotor system installed at the discharge end. The magnetic rotor, which is positioned within a separately rotating non-metallic drum, revolves at around 3500 RPM during operation while the outer drum cover rotates at the speed of the Eddy currents' belt conveyor. As the Eddy current system's rotor spins at these high speeds, an electric current is induced into conducting metals. The induced electric current produces a magnetic field that opposes the field created by the rotor, repelling the conducting metals over a pre-positioned splitter plate. The remaining MSW will simply free-fall over the rotor and will be fed to a Tomra Autosort Color machine, thus separating from the repelled non-ferrous metals. The machine uses a combination of laser and near-infrared (NIR) detection technologies to enable the separation of glass from the MSW. It also classifies the glass by color

with a high-performance camera and separates any impurities from it, thus leading to higher-quality glass that can be sold for a higher price. Because of the cost of on-site removal of glass and metals from MSW during feedstock preparation, alternatives to onsite sorting can be considered.

Shredded MSW exhibits a surface area that facilitates the reactions that happen within the gasifier. To determine a shredder that would be suitable for our MSW stream post metal and glass separation, our group reached out to Shouyu Machinery via Alibaba.com for a recommendation. We were recommended to use a single shaft shredder, followed by a double shaft shredder, both of which can be assembled in a single equipment. The single shaft shredder is equipped with a hopper, one shaft with rotary blades, a hydraulic-driven pusher arm, and a screen underneath the rotating shaft. The double shaft shredder consists of a hopper, two shafts of blade, and lacks a hydraulic pusher. The MSW will first proceed to the double shaft shredder, where the two shafts of cutting blades hook the material and then bite it to smaller pieces. The resulting MSW will then proceed to a single shaft shredder within the assembly. Here, the hydraulic driven arm will push the MSW from the hopper towards the cutting shaft to ensure that the material is sufficiently shredded by the rotary cutting blades. The MSW will be shredded until it's small enough to pass through a screen of 1cm mesh. According to our contact at Shouyu Machinery, the combined shredder system will have specifications shown in Table 5.2-1.

Table 5.2-1: Design specifications for combined shredder system.

Component	Unit	Value
2-Shaft Shredder Power	kW	150
2-Shaft Shredder Cost	USD	$68,000
Single Shaft Shredder Power	kW	180
Single Shaft Shredder Cost	USD	$10,000
Combined Rotor Length	m	2.5
Combined Cost	USD	$168,000
Combined Power Consumption	kW	330

Screw conveyors were chosen for our system due to the simplicity of their design. The length of screw conveyors between the magnetic drum separator, the Eddy current separator, and the Autosort Color was designed to be 3.048 meters based on typical distances between separation steps in material recycling facilities (Monterey Park, n.d.). A length of 6.096 meters for the screw conveyor delivering MSW from the storage pit was chosen with the assumption that the depth of our storage pit will be 4.572 meters at best. This depth is based on typical depths of MSW storage pits (EPA, n.d.). The screw conveyor delivering MSW to the shredder is 6.1 meters because the combined shredder system will be 5 meters tall. The extra 1.1 meters will facilitate MSW delivery to the hopper of the shredder. The length of the screw conveyors delivering shredded MSW to the gasifiers was based on the height of each of the gasifiers

relative to the height of the shredder system and 2 meters of distance that was deemed sufficient to separate the two processes.

5.3 Gasifier Design

The first step in the design of our gasifier was to determine the type of gasifier to use. Due to the moisture content of our raw MSW feedstock, we were limited to an updraft fixed bed gasifier. This is because updraft fixed bed gasifiers can tolerate a water content up to 60% by mass. Downdraft fixed bed gasifiers, which are closest to updraft fixed bed gasifiers in terms of tolerable water content, can only tolerate a maximum water content of 25% by mass (Basu, 2010). As shown in Figure 5.3-1, in an updraft fixed bed gasifier, the gasification agent (air in Figure 5.3-1) travels upward while the bed of fuel moves downward. The syngas leaves from the top, and the MSW feed is fed from the top. The gasifying agent enters the bed through a grate or a distributor on the side.

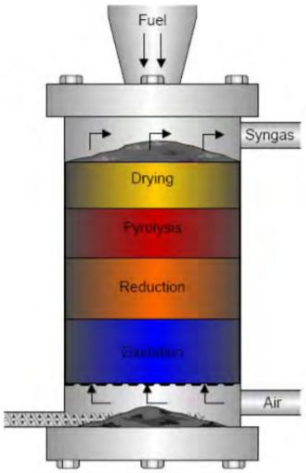

Figure 5.3-1: Updraft fixed bed gasifier (Golam, 2010).

After the type of gasifier to be used for our purpose was determined, we proceeded with modeling and simulating the process of gasification. For this purpose, we used ASPEN Plus

V11. To begin the modeling and the simulation, we first had to choose a property method for our model. To account for the non-idealities and the elevated temperature at which updraft fixed bed gasifiers operate, we chose the Redlich-Kwong Soave equation of state with the Boston-Mathias modification (RKS-BM). After specifying the property method, we had to specify the components that would be present in our simulation.

Tars were specified as naphthalene following the work of Lopamudra et al.. MSW was specified as a non-conventional component, and we based its proximate and ultimate analysis on the work of Golam. Ash was specified as a non-conventional component. We also used HCOALGEN and DCOALIGT as the enthalpy model and density model for both our MSW feedstock and the ash, respectively. The rest of the components in our simulation were specified as conventional components.

After specifying the components, we had to specify the operating temperature and pressure of our gasifier. Following the work of Begum et al., we chose an operating temperature of 700°C to maximize the ratio of CO composition to CO_2 composition in our syngas. We chose a pressure of 5 bar absolute as the operating pressure to account for the subsequent pressure drop that occurs downstream of our WTE process (see section 5.4-5.6).

After choosing operating conditions, we had to decide what approach we would follow to model our gasifier. There are two main approaches that can be followed using ASPEN Plus V11, namely: a kinetic approach, and a thermodynamic equilibrium approach (Basu, 2010). The equilibrium approach predicts maximum achievable yield of the syngas from the reactions that occur within the gasifier. The approach is based on the assumption that the residence time is long enough to allow the chemical reactions that occur within the gasifier to reach equilibrium. Furthermore, it is based on the minimisation of Gibbs free energy at equilibrium. The kinetic

approach considers that realistically, only a finite time is available for the reactions within the gasifier to occur. The model bases syngas yield and composition on reaction kinetics and reactor hydrodynamics (the physical mixing process within the gasifier). According to the work of Begum et al., the equilibrium model is suitable for temperatures above 650°C. Because our operating temperature is 700°C, we chose the equilibrium approach. After determining what approach our model would follow, proceeded with constructing the model in ASPEN.

To construct our model in ASPEN, we largely followed the work of Begum et al., which modeled the process based on four stages: drying, pyrolysis, gasification, and combustion. This resulted in the process flowsheet in Figure 5.3-2.

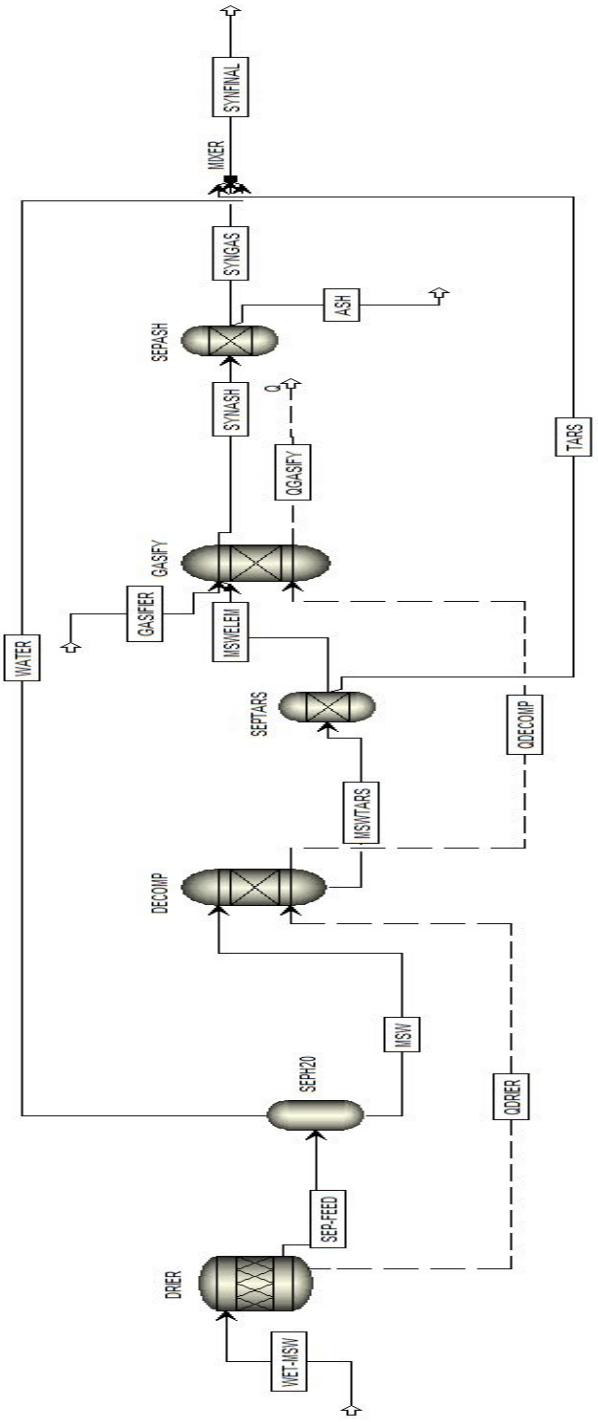

Figure 5.3-2: ASPEN Plus V11 process flowsheet of gasifier model. Heat streams have dashes.

During the drying stage, the moisture in the MSW feed to the gasifier is removed. To model drying, we used RStoic. Although drying of MSW is not a chemical reaction, RStoic, labeled as DRIER in Figure 5.3-2, allows us to convert a portion of the MSW to water. The equation $wet\ MSW \rightarrow 0.0555084\ H_2O$ was used as the drying equation based on the work of Begum et al., and a fractional conversion of 0.375 was used to reflect the 37.5 % water content by mass in the MSW feed to the gasifier. The product of drying, SEP-FEED in Figure 5.3-2, was 37.5% water by mass and the rest of the content was MSW. A separator, labeled as SEPH2O in Figure 5.3-2, was used to separate the water in stream SEP-FEED from the MSW in it. We assumed complete separation because at our operating conditions, all the moisture in our MSW evaporates according to the phase of water at our operating conditions according to steam tables from The Engineering Toolbox. The water separated from the wet MSW, labeled WATER in Figure 5.3-2, was mixed with the syngas produced to reflect the actual operation of a gasifier where the evaporated water comes off the gasifier as part of the syngas formed. It is due to this that our syngas has a high water content by mass. Because MSW was dry after the drying stage, we had to update its attribute for moisture in its proximate analysis to reflect the drying that occured. The proximate analysis of dry and wet MSW shown in Table 5.3-1 was used based on the work of Golam. Dry MSW and any heat produced from drying, labeled MSW and QDRIER in Figure 5.3-2, respectively, were fed to the pyrolysis stage.

Table 5.3-1: Proximate analysis of wet and dry ash-free MSW (Golam, 2010).

Content (%)	Wet MSW	Dry MSW
Fixed Carbon	21.7	21.7
Volatile Matter	78.3	78.3
Ash	0	0
Moisture	61.2	0

Pyrolysis involves the thermal breakdown of larger hydrocarbon molecules of MSW into smaller condensable and noncondensable gas molecules without a reaction with a gasifying agent. To model pyrolysis in ASPEN, we used RYield. RYield converts the MSW into its components including carbon, oxygen, nitrogen, hydrogen, and sulphur by specifying the yield distribution according to the ultimate analysis of the MSW in Table 5.3-1. During pyrolysis, tars are formed via the condensation of the condensable vapor produced during the process. We considered the tars formed to be 15% by mass of the feed to the pyrolysis stage based on typical tar generation rates within updraft fixed bed gasifiers (Molino et al., 2016). This reduced the carbon and hydrogen content in the ultimate analysis used for our MSW as shown in Table 5.3-2. Tars were modeled as naphthalene because its (naphthalene) structure is a good representation of the makeup of tars (Lopamudra et al., 2020). Tars leave the product of pyrolysis as soon as they are formed and exit the gasifier with the syngas formed. To account for this, we used a separator, denoted SEPTARS in Figure 5.3-2, to separate the tars from the products of pyrolysis, and complete separation was assumed. The stream of tars, labeled TARS in Figure 5.3-2, was mixed with the syngas and the water from drying to reflect actual operation of the gasifier where tars leave with the syngas formed.

Table 5.3-2: Mass composition of pyrolysis product, excluding ash that was 14.5% by mass of MSW feed.

Component	Mass composition (%)
S	0.0022
O	45.3
N	4.36
H	5.76
C	29.4
Tars	15.0
Total	100

After separating the tars from the pyrolysis product, the stream of tars-free MSW and any heat generated from pyrolysis was sent to the gasification stage. In Figure 5.3-2, the tar-free stream is labeled MSWELEM and the heat is labeled QDECOMP. During the gasification stage, steam, the gasifying agent, reacts with the products of pyrolysis to form syngas. To model the set of reactions that occur during the gasification stage, we used an RGibbs reactor. RGibbs forms syngas by minimizing Gibbs free energy, thus enforcing our equilibrium approach. In setting up the RGibbs reactor, we selected the option to calculate chemical equilibrium and phase equilibrium at the operating temperature and pressure of our gasifier. Steam was fed as the gasification agent because it is easily obtainable and cheaper relative to pure oxygen and lacks the nitrogen content of air that reduces the heating value of the resulting syngas (Yong et al., 2017). Steam was fed as 10% of the feed to the gasification stage minus the ash following the work of Begum et al., where a 0.1 equivalent ratio (the ratio of gasifying agent to feed to the

gasification stage) maximized the ratio of CO to CO_2 yield. We specified a heat stream (QGASIFY in Figure 5.3-2) coming off the gasification stage because gasification using steam is overall exothermic (Yong et al., 2017).

Table 5.3-3: Composition of product of gasification, labeled SYNGAS in Figure 5.3-2.

Component	Mass Flow (kg/hr)
H_2	149
NH_3	0.45
CH_4	424
N_2	217
CO	1,490
H_2S	11.1
CO_2	1,590
H_2O	3,390
Tars	711
Total	7,983

Although the composition of MSW post drying was based on dry ash-free MSW, MSW is commonly composed of 14-17% ash by mass (Golam, 2016). We declared the ash as 14.5% by mass of the feed to the design. We also specified it as a separate component because the composition of MSW post drying was based on that of ash-free sorted MSW. Ash settles at the bottom of the gasifier and has to be withdrawn to avoid its accumulation, which causes operational problems within the unit. To model this in ASPEN, we used a separator (labeled SEPASH) to separate the ash (labeled ASH) from the syngas formed and assumed complete separation of the ash. Following gasification, the next stage in the gasification process is

combustion. This stage serves to convert any MSW that remains unreacted after the gasification stage. Our product from the gasification stage had no residual carbon, indicating that all our MSW had reacted during the gasification stage. Due to this, we did not need to design a combustion stage.

Our model is net exothermic because heat generated from the gasification stage is greater than the heat needed for drying and pyrolysis by 0.49 MW, and the gasifier contains insulation that contains all the heat released from the process. However, heat is initially required to kickstart the drying and pyrolysis stages, both of which precede the gasification stage within the process of gasification. Due to this, an external source of heat will still be required to heat our gasifiers to the operating temperature. Natural gas will be heated in a furnace that comes with the gasifier to generate the heat needed.

After we acquired the results of our gasification system, we proceeded with designing the physical gasifiers that would fit our purpose. The first step in doing so was to size the gasifiers. To do so, we used a hearth load, which is a metric that indicates the quantity of MSW that can be processed by a gasifier over a period of time (Basu, 2010). The hearth load can be calculated according to Equation 5.3-1.

$$Hearth\ load\ (\frac{kg}{m^2 h}) = \frac{Mass\ of\ MSW\ gasified\ per\ hour}{Cross\ sectional\ area\ of\ gasifier}$$

Equation 5.3-1: Hearth load of an updraft gasifier.

The hearth load of updraft fixed bed gasifiers is typically 150 $\frac{kg}{m^2 h}$ (Basu, 2010). Considering the typical hearth load of an updraft fixed bed gasifier and the MSW feed rate to our process, we determined that we would need a gasifier with a diameter of 8.2 meters (see sample calculation in Appendix). However, the diameter of an updraft gasifier cannot exceed 4 meters because over

that, operational problems arise (Basu, 2010). Due to this, we chose a diameter of 4 meters for each of our gasifiers. As a result, each of our gasifiers can handle a maximum of 1885.7 kg/hr and a 25% increase in MSW feed rate or generation in Boulder, Colorado. The height of an updraft gasifier can be related to its diameter by a ratio of 3:1 (Basu, 2010). Based on this, we determined the height of each of our gasifiers to be 12 meters.

5.4 Syngas Cleanup

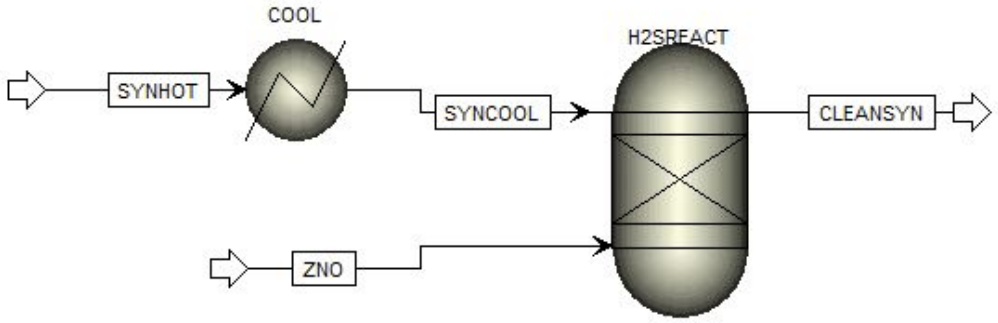

Figure 5.4-1: ASPEN Plus V11 process flow sheet for syngas cleanup

Before entering the syngas cleanup reactor, the syngas coming off the system of gasifiers must be cooled to an optimal conversion temperature, which ranges from 400-475°C (Marcantonio, 2002). Because both this reactor and the next reactor in the process (a reactor for the WGS reaction) can achieve desired conversion at 400°C, we decided to operate at this temperature to avoid using another heat exchanger between the two units. The heat exchanger (labeled as COOL in Figure 5.4-1) was used to calculate the associated heat duty. We used hot water as the cooling fluid for this heat exchanger, entering the shell at 2,260 kg/hr and 184°C and exiting as steam at the same temperature and flow rate. We designed a centrifugal pump using

ASPEN to pressurize the hot water used for this heat exchanger, as well as for the hot water used in WGS reactor (see section 5.5). To model the pump using ASPEN, specifications for 0.5 bar pressure increase and 3,140 kg/hr of hot water through the pump, ASPEN calculated an energy requirement of 76 W.

According to BASF, 30% excess zinc oxide is needed for sulfur removal in the reactor. Based on this recommendation, the molar ratio of hydrogen sulfide to zinc oxide (shown in Equation 5.4-1) and the amount of hydrogen sulfide present in the syngas stream coming off of the gasifier (stream S-119), the amount of zinc oxide needed was determined to be 275,400 kg/year. Realistically, the sorbent will be packed in the reactor prior to feeding the syngas stream (labeled SYNCOOL in Figure 5.4-1). To model this in ASPEN, we designed the reactor to treat zinc oxide as an inlet stream (labeled ZNO in Figure 5.4-1). Although the reaction occurring between the particles and syngas is slightly exothermic with 6,800 W of heat being produced, the heat released into the stream has a negative effect on temperature.

The void fraction in the reactor was calculated using Sadegh-Vaziri and Babler's correlation for spherical particles in a packed bed, shown by Equation 5.4-1. In the equation, ε is the void fraction, D_R is the reactor diameter, and D_P is the particle diameter. The combined volume of both reactors (including a void space of 0.39) was calculated to be a total of 80.48 m^3, resulting in an individual reactor size of 40.24 m^3

$$\varepsilon = \frac{1.74}{((D_R/D_p)+1.14)^2} + 0.39$$

Equation 5.4-1: Void fraction correlation for packed bed reactors

$$ZnO_{(s)} + H_2S_{(g)} \rightarrow ZnS_{(s)} + H_2O_{(g)}$$

Reaction 5.4-1: Zinc oxide sorbent reaction with hydrogen sulfide

We used the Ergun equation, shown by Equation 5.4-2, to determine the sizing of the reactor and the pressure drop over the two reactors in series. In this equation, ΔP is the pressure drop, L is the reactor length, D_P is the particle diameter, v_s is the fluid superficial velocity, ε is the bed void fraction, μ is the fluid dynamic viscosity, and ρ is the fluid density. We had to minimize pressure drop to determine optimal reactor dimensions and avoid energy-intensive compression. To do this, we used Google Sheets, and varied reactor length, particle diameter, and reactor diameter versus pressure drop, using Equation 5.4-2. We varied particle diameter up to 10 mm and found that a larger particle size yields a smaller pressure drop, as shown in Figure 5.4-1.

$$\Delta P = \frac{150\mu L}{{D_P}^2}\frac{(1-\varepsilon)^2}{\varepsilon^3}v_S + \frac{1.75L\rho}{D_P}\frac{(1-\varepsilon)}{\varepsilon^3}v_s|v_s|$$

Equation 5.4-2: Ergun equation used for sizing and pressure drop

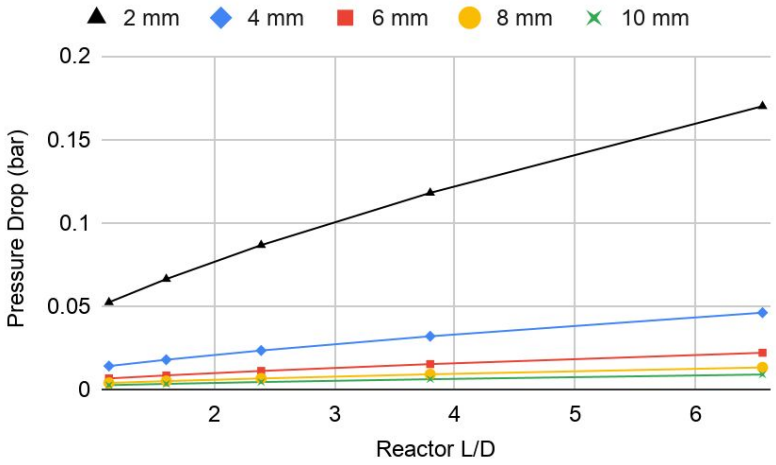

Figure 5.4-1: Reactor length/diameter versus pressure drop for a packed bed reactor with various spherical particle diameter sizes

As shown in Figure 5.4-1, the pressure drop for a particle with a diameter between 6 mm to 10 mm is similar. We chose a particle size of 6 mm to result in a higher ratio of length to particle diameter, which is more likely to satisfy that requirement for packed bed reactors (Davis & Davis, 2013). To determine reactor dimensions, we iterated diameter while limiting length and

pressure drop. To avoid an extreme reactor length requiring high cost, we limited the length of each reactor to be no more than double the reactor diameter. The final results are shown in Table 5.4-1.

Table 5.4-1: Ergun equation results to minimize pressure drop

Variable	Units	Value
Pressure Drop	bar	0.015
Reactor Length	m	5.7
Reactor Diameter	m	3
Particle Diameter	m	0.006

5.5 Water Gas Shift Reaction

The outlet stream from syngas cleanup underwent a water-gas shift reaction to convert CO and H_2O into CO_2 and H_2 , thus increasing the amount of H_2 entering the SOFC. Although SOFCs can operate with different fuel sources, increasing the amount of H_2 in the feed increases the efficiency of internal reactions and reduces thermal stress on the system (Speight, J. 2016).

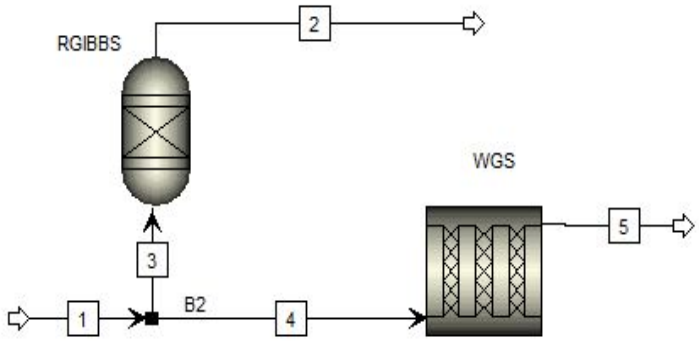

Figure 5.5-1: ASPEN Plus V11 process flowsheet of water-gas shift reaction model

The reaction was modeled based on a high-Temperature shift (HTS) catalyst-based reactor. The catalyst used is an iron oxide – chromium oxide-based catalyst from the model developed by Adam and Barton that confirmed it to be the most commonly used catalyst industrially (Barton, P. 2009). Iron oxide-chromium oxide was chosen as the catalyst based on its superior performance relative to three other common industrial HTS catalysts. The catalyst consists of 88% Fe_2O_3, 8% Cr_2O_3, and 4% CuO. The density of the catalyst was calculated by adding the product of the density of each component and its (the component's) percentage weight composition. A sensitivity analysis on the reactor was carried out in ASPEN to determine the required amount of catalyst weight. This analysis was based on the relationship between the reactor temperature, the catalyst weight, and CO conversion at equilibrium conditions. Following this analysis, we determined that the catalyst weight required to achieve the reaction is 4000 kg at a reactor temperature of 400°C. Under these conditions, the CO conversion was determined to be 87.8%. The void bed was determined to be 0.4 using equation 5.4-1. The pellet diameter was specified as 9 mm based on the common pellet size industrially. The reaction was modeled and simulated in ASPEN based on an industrial rate expression in the work of Lima et al., which is shown in Equation 5.5-1.

$$r = k_0 \cdot e^{-\frac{Ea}{RT}} \cdot P^{l}_{CO} \cdot P^{m}_{H_2O} \cdot P^{n}_{CO_2} \cdot P^{q}_{H_2} \cdot \left(1 - \frac{1}{Keq} \cdot \frac{P_{CO_2} P_{H_2}}{P_{CO} \cdot P_{H_2O}}\right)$$

Equation 5.5-1: Industrial water gas shift reaction rate expression.

In equation 5.5-1, r represents reaction rate, k_0 is a pre-exponential factor, E_a is the activation energy, R is the universal gas constant, T is absolute temperature, K_{eq} is a reaction equilibrium constant, P_i is the partial pressure of reaction component i, and l, m, n, and q are parameters estimated from experimental data. Table 5.5-1 shows these parameters as they were

determined by Adams and Barton along with the calculated equilibrium constant at the operating temperature of 400°C.

Table 5.5-1: Value of parameters as determined by Adams and Barton

K_{eq}	k_0	E_a(kJ/mol)	*l*	*m*	*n*	*q*
11.7	25	110	1	0	-0.32	-0.083

The parameters in Table 5.5-1 were used in setting up an RPlug reactor in ASPEN, which is the reactor we used to model the water-gas shift reaction in ASPEN. We also ran a secondary simulation using an RGibbs reactor to compare results from the RPlug reactor and to also ensure that the reaction was occurring at equilibrium at the specified parameters. In the RPlug reactor, we specified the reaction as a general reaction and classified it as a power law reaction. In the reaction section, the water-gas shift reaction was specified according to the reaction expression in Reaction 5.5-1.

$$H_2O + CO \leftrightarrow H_2 + CO_2$$

Reaction 5.5-1: Water-gas shift reaction

To avoid the need for a heat exchanger between syngas cleanup and the water-gas shift reaction units, we specified the reactor temperature as 400°C, which is equivalent to the reactor temperature for syngas cleanup. We specified the reactor pressure as 3.5 bar to based on the system pressure profile to maintain gas flow. A simulation of the reactor yielded a pressure drop of 0.04 bar and we validated the value using the Ergun equation (Equation 5.4-1). Because the water-gas shift reaction is exothermic, the reactor was constructed in a shell and tube heat exchanger style to maintain operation under isothermal conditions. The pellet size and void space of the catalyst were used to calculate the reactor tube volume (see Appendix for calculation). The

reactor diameter was specified to be 10 cm to minimize operational problems arising from an increase in pressure drop due to a specific decrease in tube diameter . The number of tubes was calculated by dividing the tube volume by the tube area that was calculated using the tube diameter. Table 5.4-2 shows a summary of the reactor specifications.

Table 5.5-2: WGS reactor specifications

Parameters	Units	Value
Tube Diameter	cm	10
Tube Length	m	1.7
Number of Tubes	N/A	160
Bed Void	N/A	0.40
Pellet diameter	mm	9.00
Reactor geometry area	m^2	85.45
Reactor duty area	m^2	75.15

The duty of the reactor was determined from ASPEN to be 0.49 MW. The calculated area of the heat exchanger using the dimensions of the reactor had to be greater than the area calculated using the heat duty of the heat exchanger to ensure that the designed area can contain the reactor heat transfer. We calculated the area of the reactor geometry to be 85.45 m^2 using the geometry of the reactor, and the area duty to be 75.15 m^2 using the heat duty collected from ASPEN and the correlation for calculating heat exchanger area (see Appendix for calculation). The overall heat transfer coefficient was estimated to be 30 W/m^2k following the work of Peters, Timmerhaus & West, and the mean temperature was calculated to be 216°C. Boiling water was used to cool off the excess heat produced by the reaction. The water was fed to the reactor shell at 184°C at a rate of 2,200 kg/hr, and exited as steam at the same temperature and rate.

5.6 Solid Oxide Fuel Cell and Heat Recovery

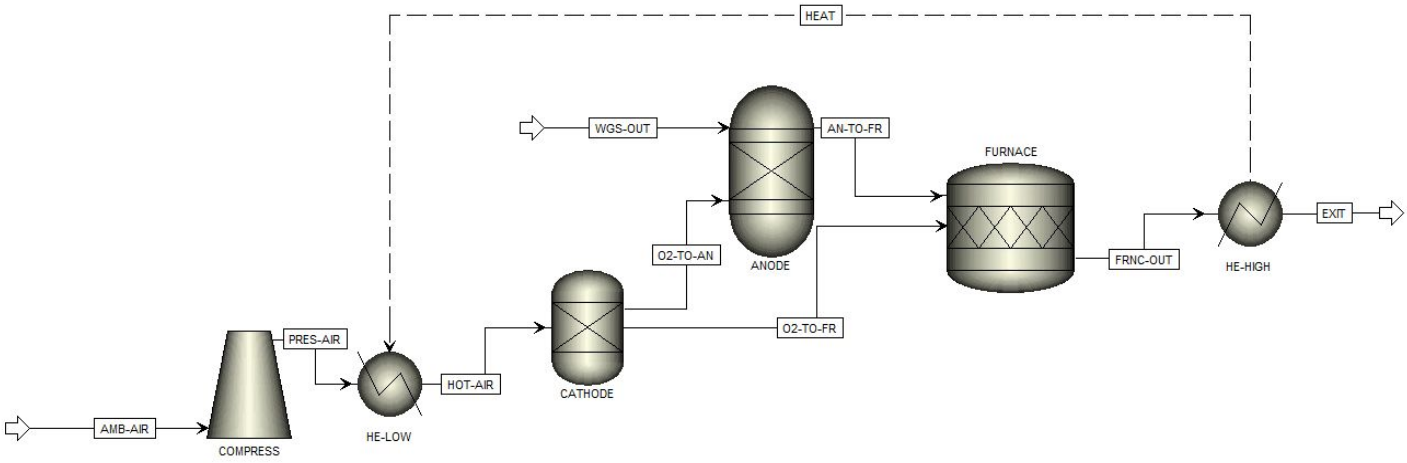

Figure 5.6-1: ASPEN Plus V11 flowsheet of SOFC model

Following the approach taken by Zhang, we modeled the SOFC as depicted in Figure 5.6-1. The syngas (labeled as WGS-OUT in figure 5.6-1) was fed directly to the anode (labeled as ANODE) of the fuel cell, where the following electrolytic reactions occur:

$$H_2 + O^{2-} \rightarrow H_2O + 2e^- \ (1)$$

$$CO + O^{2-} \rightarrow CO_2 + 2e^- \ (2)$$

$$CH_4 + 4O^{2-} \rightarrow 2H_2O + CO_2 + 8e^- \ (3)$$

Equation 5.6-1: Electrolytic Reactions

To supply oxygen, ambient air (stream labeled AMB-AIR) was compressed (block labeled COMPRESS) and introduced to the cathode (labeled CATHODE), which we modeled as a separator. At the cathode, the oxygen interacts with the interface according to reaction 5.6-2:

$$O_2 + 4e^- \rightarrow 2O^{2-} \ (4)$$

Equation 5.6-2: Oxygen Reduction

Because ASPEN is incapable of handling electrolytic reactions, we selected an equivalent set of reactions to imitate this process. These reactions, shown below, include methane reformation and the water-gas shift reaction:

$$CO + H_2O \rightarrow CO_2 + H_2 \ (5)$$

$$CH_4 + 2H_2O \rightarrow CO_2 + 4H_2 \ (6)$$

$$2H_2 + O_2 \rightarrow 2H_2O \ (7)$$

Equation 5.6-3: Shifted Reactions

The reformation and water-gas shift reactions are thermodynamically favored over their electrolytic alternatives at the operating temperature, making the shift from equations 1-4 to 5-7 quite valid. Assuming equations 5-6 to be prominent over their electrolytic counterparts, hydrogen was assumed as the only species that reacts electrolytically. All other electrolytically reactive species were considered to be hydrogen equivalents in the model. We modeled the anode using an RGibbs reactor to allow thermodynamic equilibrium to be reached before ejecting spent fuel.

As stated, we modeled the cathode as a separator to simulate the diffusion of anionic oxygen (labeled O2-TO-AN) across the electrolyte. The rate of this diffusion is dependent upon the thermodynamic properties of the air and feedstock, as well as material properties and dimensions of the fuel cell. The fuel utilization is also determined by these properties, which are out of scope. Because the utilization was unknown, we selected a reasonable fuel utilization of 85%, which is the efficiency that optimized Zhang's model. We defined the utilization factor with respect to the hydrogen content of the syngas and its equivalents according to Equation 5.6-4.

$$n_{H_2(consumed)} = U_f \cdot n_{H_2(eq.)} = U_f \cdot \left(n_{H_2} + n_{CO} + 4n_{CH4} \cdots \right)$$

Equation 5.6-4: Equivalent consumption of hydrogen

Note that n is defined by the molar flow of the species in its subscript, while U_f is the fuel utilization as a fraction. Considering stoichiometry of oxygen with hydrogen, this expression translates into the oxygen diffusion rate according to Equation 5.6-5.

$$n_{H_2(consumed)} = 2n_{O_2(diffused)}$$

Equation 5.6-5: Equivalent consumption of oxygen

The furnace downstream of the fuel cell (labeled FURNACE in Figure 5.6-1), serves a dual purpose: combusting all remaining hydrocarbons in the spent fuel and burning tars, which were assumed inert in the fuel cell. The unspent fuel (stream labeled as AN-TO-FR) and the undiffused air (stream labeled as O2-TO-FR) streams were fed to the furnace to simulate a combined stream leaving the fuel cell. Combustion of naphthalene was designated within the furnace since the tars were modeled as this component. The furnace was assumed adiabatic to account for insulation of the unit, which maximized the potential for heat loss recovery downstream. Oxygen was fed to the fuel cell in excess so that the remnants were enough for complete combustion of all combustibles in the furnace. The lower level concentration of oxygen for combustion was considered negligible enough to be disregarded at the extreme temperatures in our system. Common practice, however, dictates that 2% excess oxygen by mole in the stack gas is required to account for nonuniform mixing, and the feed was specified as such. The exhaust (stream labeled as FRNC-OUT) from the furnace is hot enough to heat the incoming air (stream labeled as PRES-AIR) to operating temperature, simulated through HE-HIGH and HE-LOW, yet still remain a significant source of heat to be recovered.

The ASPEN model reported the total energy output of the fuel cell, but gave no figures on the electrical power or efficiency. For these variables, the current and voltage had to be determined. Given information on the consumption of oxygen in the anode, the current was readily evaluated according to Equation 5.6-6.

$$I = 4F \cdot n_{O_2(diffused)}$$

Equation 5.6-6: Current from hydrogen consumption

The coefficient (4) in Equation 5.6-3 arises from the stoichiometry of the electrolytic reaction. To find an appropriate voltage curve, we consulted the DoE Fuel Cell Handbook. Empirical correlations exist that relate the voltage at chosen operating conditions to a reference curve at others. The total voltage is a sum of terms relating to conditions in the electrodes, temperature, pressure according to Equation 5.6-7.

$$V_{total} = V_{anode} + V_{cathode} + V_{temp.} + V_{pressure}$$

$$\therefore V = V_{ref} + \Delta V_{anode} + \Delta V_{cathode} + \Delta V_{temp.} + \Delta V_{pressure}$$

Equation 5.6-7: Determining voltage from reference curve

The appropriate correlations were used as applied to the change in each term (see Appendix for calculations involving the terms). A series of trial and error tests were conducted to determine the voltage and the corresponding current density, allowing the number of stacks to be determined.

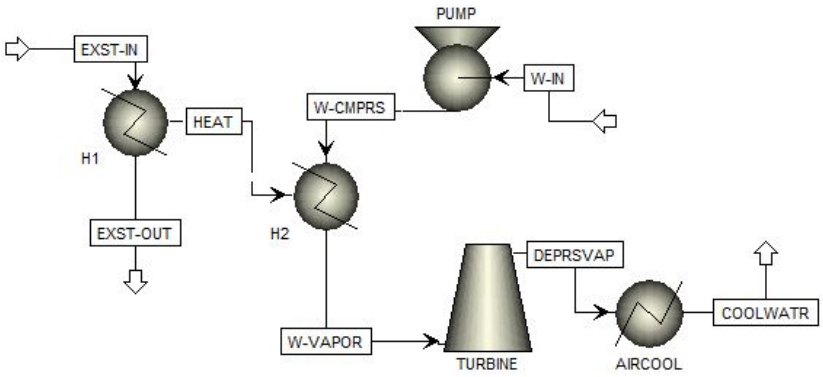

Figure 5.6-2: ASPEN Plus V11 flow sheet showing model of Rankine cycle.

Downstream of the fuel cell, a Rankine Cycle was designed as in figure 5.6-2 for the purpose of recovering heat waste from the exhaust (labeled EXST-IN in figure 5.6-2). Assuming an ideal cycle, we optimized the power according to an energy balance that factored in the Carnot Efficiency according to Equation 5.6-8.

$$P = n_{exhaust} C_{P(exhaust)} \left(T_{in(exhaust)} - T_{water(hot)} \right) \left(1 - T_{water(cold)} \div T_{water(hot)} \right)$$

Equation 5.6-8: Rankine cycle energy balance.

Note that $n_{exhaust}$ refers to the the molar flow rate of the furnace exhaust, while $C_{P(exhaust)}$ refers to its heat capacity. The subscripts *hot* and *cold* refer to the temperature extremes of the water within the cycle. To bring the expression into a solvable format, the outlets of the heat exchanger were assumed to converge upon the same temperature (see Appendix). Though this approach does not replicate the design exactly, it bears results within a reasonable range of optimal power. The optimal temperature of water exiting the heat exchanger (stream W-VAPOR) was determined to exist within the supercritical regime (see Appendix for calculations). We made a judicious decision to maintain this temperature just below the supercritical point, such that isobaric expansion gave a saturated vapor (366°C and 200 bar at equilibrium). We designed the

heat exchanger (modeled as heaters H1 and H2) to superheat the steam by a few degrees over this equilibrium point, ensuring complete vaporization. The set point for the heat stream (HEAT) was an arbitrary exhaust exit (EXST-OUT) temperature of $390^{o}C$. Then, we selected a diaphragm pump (block labeled PUMP) for the compression of water (stream W-IN compressed to W-CMPRS) due to its operating range, which may compress in excess of 1,000 bar (PumpScout). Upon superheating, this stream was fed to a rotary turbine (block labeled TURBINE) to simulate the conversion of thermodynamic potential to mechanical work. Condensation, as mentioned, was assumed to occur along a vast surface area, allowing the liquid-vapor mixture (stream DEPRSVAP) to return to a liquid at ambient conditions (stream labeled as COOLWATR). To model this ambient heat carryoff, this section of piping was simulated as a condenser (block labeled AIRCOOL) with the outlet conditions specified. Note that the thermodynamic properties of streams W-IN and COOLWATR are equivalent as well as their flow rates, such that they model a recycle stream, though not explicitly shown. The flow rate of this stream was set through a sensitivity analysis that satisfied superheating of the steam leaving the heat exchanger (stream W-VAPOR).

5.7 Carbon Capture

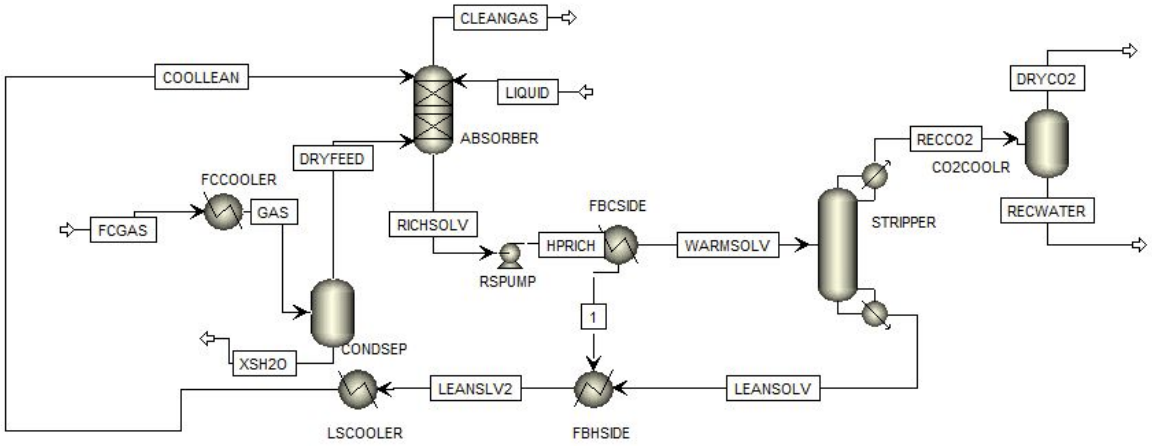

Figure 5.7-1: ASPEN Plus V11 flowsheet of carbon capturing process

A carbon capturing process was designed to capture the carbon dioxide produced during the process, thus reducing greenhouse emissions from our process to the environment. The process is made up of two main steps: a packed bed absorption column (labeled ABSORBER in Figure 5.7-1) that absorbs the produced CO_2 using monoethanolamine (MEA) solvent, and a stripping column named (labeled STRIPPER) that strips out the CO_2 by heating the solvent. To model these steps in ASPEN, we used the electrolyte nonrandom-two liquid (ELECNRTL) property method following the work of Lin et al. We used the property method in particular to account for the various ionic forms that the solvent transforms to during the process, which are shown in Reaction 5.7-1.

$$H_2O + HCO_3 \leftrightarrow CO_3^{-2} + H_3O^+$$

$$2H_2O + CO_2 \leftrightarrow HCO_3^- + H_3O^+$$

$$H_2O + MEACOO^- \leftrightarrow MOMOE^{-1} + HCO_3^-$$

$$H_2O + MEA^+ \leftrightarrow MONOE^{-1} + H_3O^+$$

Reaction 5.7-1: The absorption equilibrium reactions

We used a heat exchanger (labeled FCCOOLER in Figure 5.7-1) and a flash drum (labeled CONDSEP) to prepare the exhaust from the SOFC for absorption. Based on Petrovic & Soltani's research, the optimum temperature to minimize energy requirements for the gas entering the absorber is 50°C. The heat exchanger cooled the gas from 390°C to 50°C using cooling water that was fed at 25°C and left at 35°C at a flow of 636,300 kg/hr. A MEA to CO_2 ratio of 3:1 is desired for absorption to conducively occur. Due to this, a specific amount of MEA is needed in the solvent section to meet the ratio. Furthermore, having water flow to the solvent section reduces the amount of MEA in the section, thus reducing the quantity of CO_2 captured. To prevent this from happening, the gas must be dried before it is fed to the absorber.

To model and simulate the drying of gas, we used the flash drum. To determine the diameter of the drum, we used Equation 5.7-2, where u_{perm} is the maximum possible velocity of the vapor in ft/s, K_{drum} is an empirical constant which is assumed to be 0.35 based on the recommendation from Wankat (2016), the density of the liquid is ρ_L, and the density of the vapor is ρ_v. Based on the fluid densities and vapor volumetric flow rate obtained from ASPEN, the drum diameter and the length were both calculated to be 2.45 m.

$$u_{Perm} = K_{drum}\sqrt{\frac{\rho_v - \rho_L}{\rho_v}}$$

Equation 5.7-2: The maximum permissible vapor velocity equation (Wankat, 2016)

The dry gas (labeled DRYFEED in Figure 5.7-1) was fed to the packed bed absorption column from the bottom (stage 3) at 50°C and 2 bar, and the gas was fed from the the top of the tower at 40°C via two streams: feed stream labeled LIQUID and recycle stream labeled COOLLEAN in Figure 5.7-1. Feeding the liquid at the top of the tower and the vapor at the bottom tower is important to ensure vapor liquid interface, and hence, the reaction within the tower height. The rich solvent stream (labeled RICHSOLV in Figure 5.7-1) exits at 71°C and 1 bar and the cleaned gas stream (labeled CLEANGAS), mainly consisting of steam, water and nitrogen, exits from the top of the tower and vents to the atmosphere at a temperature of 52°C and 1 bar.

The absorber was designed in ASPEN to be a packed bed column consisting of 3 equilibrium stages, each packed with pall rings at a height of 3 m. We minimized the number of equilibrium stages required to minimize equipment cost and because 3 equilibrium stages are shown to yield 99.9% by mass of CO_2 absorbed. Pall rings were specified as the packing because they are the most commonly used packing material as they reduce liquid holdup in the column and prevent high pressure drop. The temperature (40°C) and pressure (3 bar) were specified for this column based on the recommended values found in literature to give the optimal recovery of CO_2 (Lin et al., 2011). The Height Equivalent to the Theoretical Plate (HETP) was calculated to be 3, using the packed column size correlations in Watkans (2016). The height of the column was calculated using the HETP correlation shown in Equation 5.7-3. We specified the diameter of the absorber and ASPEN calculated the pressure drop for this specification. From ASPEN, at a diameter of 2 m and packed bed height of 9 m, the pressure drop is minimal at 0.08 bar. Because this column does not have a condenser or reboiler, we assumed that the packed bed height will be the same as the reactor height.

$$HETP = \frac{Height}{Theoretical\ number\ of\ plates}$$

Equation 5.7-3: The Height Equivalent to the Theoretical Plate equation

To account for the pressure drop across the column, piping, and heat exchanger, a pump labeled RSPUMP was designed to pressurize the fluid leaving the bottoms of the absorber, labeled RICHSOLV, before entering the stripper. Immediately after exiting the pump, the solvent stream, labeled HPRICH enters a heat exchanger, labeled FBCSIDE, to raise the temperature of the solvent for the stripping column. To minimize energy requirements, we designed a cross heat exchanger which utilizes the temperature of both streams (HPRICH and LEANSOLV) as heating/cooling fluids, rather than using two heat exchangers to heat/cool. HPRICH stream was used to cool off the LEANSOLV stream. In ASPEN, this was modeled with two heat exchangers by sending a heat stream from heat exchanger FBCSIDE to heat exchanger FBHSIDE.

Heat exchanger FBCSIDE heats the rich solvent (labeled RICHSOLV) stream from 71°C to 125 °C before it is fed to the stripping column. Our rich solvent was heated to 125°C based on Warudkar's (2013) correlation between stripping temperature and column diameter requirement. The normal operating temperature for stripping columns is between 100°C-110°C. However, because our column is operating at a pressure below normal stripping pressure (1.3 bar), an increase in temperature results in a decrease in pressure requirement and decrease in column diameter (Warudkar, 2013). This is important because minimizing diameter requirement decreases the bare module cost of the column. The rich solvent was fed to the tray-based stripper column at stage 2 (at the top) to reflect the actual operation of the stripping column where the rich solvent (labeled WARMSOLV) enters at the tray below the condenser.

According to Seader et al., a column diameter less than 0.7 m is desired to lower pressure drop and increase efficiency. However, reducing the column diameter increases the column height and the number of trays, increasing cost of the equipment and associated safety hazards. To account for this, a 1 m diameter was specified to minimize column height and the number of trays needed. With these specifications, ASPEN calculated a tray spacing of 0.6 m, a column height of 4.88 m, and a pressure drop of 0.46 bar. Based on a trial and error analysis we carried out in ASPEN, we determined that the stripper required 10 stages to achieve optimal CO_2 recovery. The 10 stages include a kettle reboiler, a partial condenser, and 8 sieve trays. Peters et al. suggest adding 3 meters to the height of the stripper to take the condenser height (1 meter) and reboiler height(2 meters) into account for a 1 m diameter column. Considering this, we determined the final length of the tower to be 7.88 m.

The recovered CO_2 stream (labeled RECCO2 in Figure 5.7-1) exits the condenser at 86°C and 3 bar while the lean solvent stream (labeled LEANSOLV) exits the reboiler at 137°C and 3 bar. The area of the condenser and that of the reboiler was calculated using Equation 5.7-4, where Q is the heat duty determined from the ASPEN simulation, A is the surface area, U is the overall heat transfer coefficient, and ΔT_{LMTD} is the log mean temperature difference in the heat exchanger. According to Peters, Timmerhaus, & West, the overall heat transfer coefficient for the condenser and the reboiler can be approximated as 850 and 1100 W/m^{2}K, respectively.

$$Q = A\ U\ \Delta T_{LMTD}$$

Equation 5.7-4: Heat exchanger design equation

Before CO_2 is sent to storage, the gas must be dried and cooled (Ferrara et al., 2017). In reality, the cooling is achieved by feeding the recovered CO_2 to a heat exchanger that lowers the

temperature of the gas from 86°C to 45°C before it is sent to the drum (labeled CO2COOLR), which separates the gas from water. However, this heat exchanger was not modeled in ASPEN, and the stream was sent directly to the drum. The operating temperature of the drum was specified as 45°C to lower the temperature of the gas to the required temperature of 45°C. The heat duty obtained from the simulation of the drum in ASPEN was used to calculate the heat exchanger area needed for the cooling according to Equation 5.7-4. The drum diameter was calculated using Equation 5.7-2, and the values used for the volumetric flow rate of the vapor and density of the liquid and gases were obtained from ASPEN. The length of the drum was determined to be 1 m and the diameter to be 0.8 m. The dry CO_2 (DRYCO2) was collected and stored underground at a rate of 60,240,000 kg/year.

We recycled the lean solvent (labeled LEANSOLV) coming off the bottom of the stripper back to the absorber to increase CO_2 absorption, as the recycle stream minimizes the requirement for adding MEA and maximizes vapor-liquid interface. Because the lean solvent has to be at the same temperature as the MEA solvent (stream labeled LIQUID) before it is fed to the absorber, the lean solvent was passed through heat exchangers. First, the cross heat exchanger was used for heating the solvent coming off the absorber. In ASPEN, this lean solvent was fed to the heat exchanger labeled FBHSIDE in Figure 5.7-1, which consumes the heat from FBCSIDE, thus satisfying the energy transfer for the cross-flow heat exchanger. This heat exchanger cooled the solvent from 137°C to 82°C. The cooler lean solvent stream (labeled LEANSLV2) was then passed through the heat exchanger labeled LSCOOLER, which further cooled it from 82°C to 40°C. The cooled lean solvent stream (labeled COOLSOLV) fed to the absorber at the same stage as the make-up solvent (labeled LIQUID) stream to mix both solvent feed streams.

6. Safety, Environmental, and Societal Considerations

There are several safety and environmental hazards associated with the WTE process that we need to account for to protect plant personnel and the surrounding environment. These hazards stem from various chemicals and substances that make up our system. These substances and chemicals include carbon monoxide (CO), carbon dioxide (CO_2), methane (CH_4), hydrogen sulfide (H_2S), glass, metals, monoethanolamine (MEA), and steam. On top of that, our facility will contain a storage pit that can pose a safety hazard.

For general safety, all plant personnel will wear personal protective equipment at all times when on-site. This includes goggles, a safety hat, and reflective clothing. Furthermore, all personnel on-site will wear long pants and closed-toe shoes. Guidelines set forth by the Occupational Safety and Health Administration (OSHA) will be taught to all plant personnel. Plant personnel will also be taught about potential sources and symptoms of exposure to the various hazardous chemicals. Processing equipment generating heat will be insulated to contain the heat.

CO gas is a component of the syngas produced from the gasification of MSW. According to OSHA, the permissible exposure limit for the gas is 50 parts per million (ppm) over an 8-hour period (OSHA, n.d.). The gas is highly flammable, toxic if inhaled, causes damage to organs through prolonged and repeated exposure, and also acts as a greenhouse gas (Air Liquide, 2018). To prevent these hazards, pipes bearing CO will be constantly inspected for potential leaks. Personnel carrying out the inspections will wear respirators with appropriate canisters, in conjunction with personal CO monitoring. Seals that prevent the backflow of syngas within our gasifier system will be constantly maintained to prevent leaks. Proper ventilation will be

implemented around our gasifier system and any pipes carrying CO to accommodate any leaks. To account for potential explosions due to a fire, a flare system will be implemented to discharge CO to the atmosphere in case of a fire.

CO_2 is a component of syngas and is also produced by the WGS reaction. The primary safety concern associated with CO_2 results from its behavior as a simple asphyxiant (OSHA, n.d.). According to OSHA, the permissible exposure limit for the gas over an 8-hour period is 5000 ppm. To prevent exposure to CO_2 on-site, regular maintenance and inspection of pipes carrying the gas will be carried out. The CO_2 generated by our process will be captured and stored underground (see section 5.8). Transportation and storage of CO_2 pose additional safety hazards. Transporting CO_2 to underground storage through pipelines increases the potential for leakages. To prevent these leakages, the water content of the CO_2 under transportation will be kept low to avoid corrosion of the carbon-manganese steel used in pipe construction, which is responsible for most leakages (Ralston, 2014). Gradual CO_2 leaks from underground storage can occur if the storage site is not properly selected or prepared for storage. Gradual CO_2 leakage poses risk to fresh groundwater resources as it acidifies water, increasing its ability to breakdown the surrounding rocks and the potential for leakage into the soils or water table (Ralston, 2014). Furthermore, sudden catastrophic leakage of CO_2 from underground storage has the potential to kill humans and animals. The safety aspects of the underground storage of CO_2 are highly complex and vary depending on the geology of the site (Ralston, 2014). Due to this, a team of geologists and similar experts will be put in place to select a conducive site for storage and also manage the safety aspects of the process. However, generally, to curb potential safety and environmental risks associated with underground storage, care will be taken to properly seal storage sites.

Methane mainly poses safety and environmental hazards because it is highly flammable and also acts as a greenhouse gas. In our WTE process, methane is a component of the syngas produced via gasification and natural gas that will be used as fuel to heat our gasifier system. The permissible exposure limit to methane over an 8-hour period is 1000 ppm according to the National Institute for Occupational Safety and Health (NIOSH, 2004). To prevent associated safety and environmental hazards, methane, and any pipes carrying it will be kept away from any heat and ignition sources. The methane that will fuel our gasifier system will be properly stored in containers and kept away from any hot substances and any heat sources. Flaring systems will be put in place to discharge any methane in case of a fire close to a methane-bearing stream. Pipes will also be regularly maintained and checked for methane leaks that can contribute to greenhouse effects.

MEA will be fed to our carbon capturing process as a lean solvent. MEA is combustible, harmful when swallowed, and causes severe skin burns and eye damage (MEA Safety Data Sheet). To prevent associated safety and environmental hazards, MEA will be stored in a well-ventilated and locked up place, and its container will be tightly closed at all times. Any unused samples will be properly disposed of in appropriate waste containers. Plant personnel handling the liquid will wear face protection at all times and will do so in a well-ventilated environment. In case of any associated fires, CO_2, dry chemical, or foam will be applied for extinction.

Hydrogen sulfide is also a component of the syngas produced via gasification. The permissible exposure limit to hydrogen sulfide set forth by OSHA over an 8-hour period is 1 ppm (OSHA, n.d.). The gas is highly flammable, burns and produces other toxic vapors and gases such as sulfur dioxide when exposed to air, and also causes harm to aquatic life. To

prevent associated health and environmental hazards, our gasifier and pipes carrying the gas will be regularly maintained and inspected for leaks. Inspectors will wear respirators following OSHA guidelines at all times when doing so. Flaring systems will also be implemented to discharge the gas in case of any fires. Because the hydrogen sulfide in our system will be essentially captured during syngas cleanup, it will likely not pose any environmental hazards. The sorbent used in syngas cleanup will be properly disposed of in designated containers.

Ash (noncombustible materials) is a byproduct of gasification and will be collected from the bottom of each of the five gasification units as bottom ash. Bottom ash from MSW gasification is usually classified as non-hazardous and can thus be landfilled (Aneeta et al., 2017). The ash can also be used in construction applications as a subbase material (Aneeta et al., 2017). Due to the non-hazardous nature of the bottom ash generated from our process and the potential for it to be applied in various applications, we are assuming that we will not incur landfilling costs.

Glass and metals are part of raw MSW and will be recovered during MSW preparation (see section 5.2). All personnel working on the metal and glass recovery sections will wear cut-resistant glass. Due to the presence of a storage pit on-site, there will be great potential for accidents from pitfalls. To prevent such accidents, signs with warnings about potential risks due to falls and contact with MSW will be posted around the perimeter of the storage pit. The signs will be posted in multiple languages to account for the safety of personnel with limited English proficiency. Safety guidelines will also be implemented for people in charge of delivering the raw MSW to the storage pit.

Our plant has the potential to generate odor due to the MSW on site. This odor can potentially pollute the air on-site and also in communities surrounding our plant. We anticipate

such potential to be low because our storage site is an enclosed pit under negative air pressure that eliminates the smell.

Although various hazards are associated with our plant, we anticipate our plant to be more beneficial than hazardous to the city of Boulder, Colorado. Our plant will reduce the quantity of MSW going to landfill, thus helping the city achieve the sustainability goals it set to be achieved by the year 2025. Our plant will also generate electricity that will power neighboring communities, provide employment opportunities in the city, and improve the economy of the city and the state of Colorado as a whole.

7. Economic Analysis

Our plant is expected to generate a maximum of $31,946,552 in revenue annually. Revenue is expected to be generated from the sale of electricity, recovered metals and glass from raw MSW, and tipping fees for MSW collection. Revenue generated from tipping fees for MSW collection is based on a tipping fee of $101 per 1000 kilograms of MSW, which is the tipping fee for MSW in Boulder, Colorado. Revenue generated from the sale of metals and glass is based on a selling price of $3.3 per kilogram of scrap metal and $63.5 per 1000 kilograms of cullet glass, respectively. The aforementioned price of metals is the lowest price of a scrap metal in Colorado, and the price of glass is based on the median of typical prices for scrap cullet glass in the United States (Recycling Product News, 2017; Metal Prices, n.d). We based the price of the recovered glass on culleted glass because the AutoSort Color generates cullet glass. The price of the electricity generated by our process was based on the price of electricity in Boulder, Colorado, which is 11.05 cents per kilowatt-hour.

Table 7.1-1: Sources of revenue for our WTE plant.

Material	Annual Revenue	Basis Price
Recovered Metals	$18,110,400	$3.3/kg
Recovered Glass	$152,400	$63.5/1000 kg
MSW	$6,923,752	$101/1000 kg
Electricity	$6,438,528	11.05 cents/ kWh
Total	$31,664,680	

The cost of manufacturing for our plant is $36,192,437, which is $4,527,757 greater than the revenue we generate annually. This cost is scaled from operating costs, including operating labor costs, utilities costs, and costs associated with treating our waste streams (see sample calculations in Appendix and Tables 7.1-2 and 7.1-3 for breakdown of utility costs). Costs associated with treating waste streams account for landfilling ash, wastewater treatment, and CO_2 storage. In our analysis, the cost of landfilling ash was assumed to be $101 per 1000 kilograms, which is equivalent to our tipping fee for MSW. The total capital cost for our plant is $69,987,562. We scaled this cost from purchase equipment costs of major equipment that makes up our process using the methods employed in *Analysis, Synthesis, and Design of Chemical Processes, Fourth Edition*. We used a Lang factor of 3.63 to scale total plant capital cost from purchase equipment cost, which is the Lang factor designated for a solid-fluid processing plant. Based on a break-even analysis of our plant, it (the plant) will not generate any profits over its lifetime (see Figure 7.1-3).

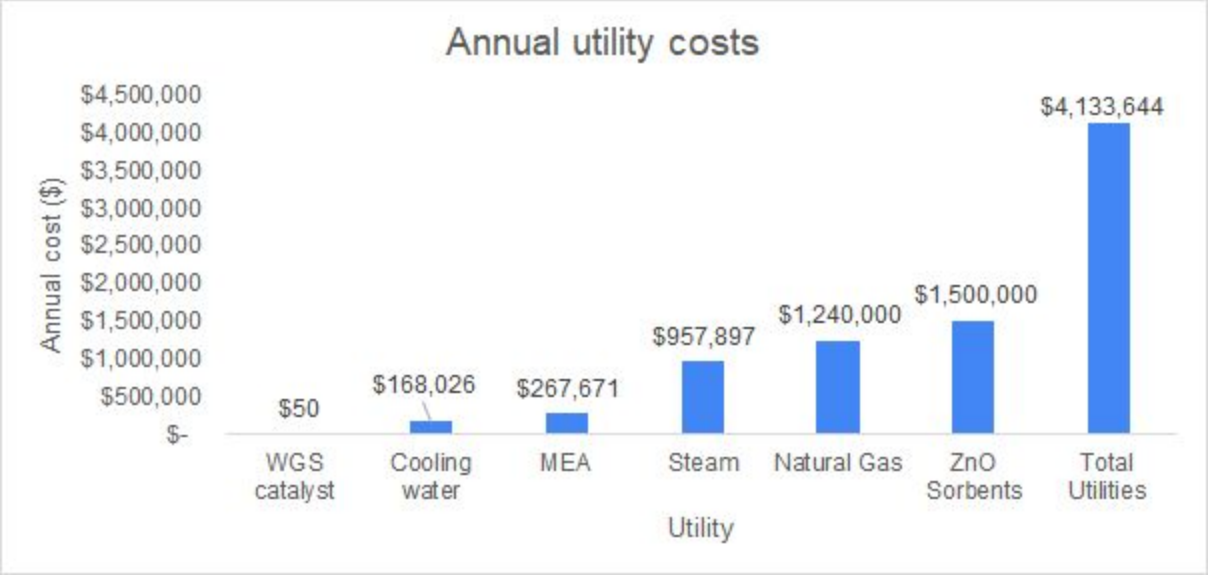

Figure 7.1-1: Breakdown of utility costs

Figure 7.1-2: Breakdown of waste treatment costs

Table 7.7-3: Summary of capital and annual operating costs.

Description	Cost
Utilities	$4,133,644
Operating labor	$3,829,196
Waste Treatment	$5,518,152
Cost of manufacturing (COM)	$36,192,437
Total plant capital cost	$69,987,562

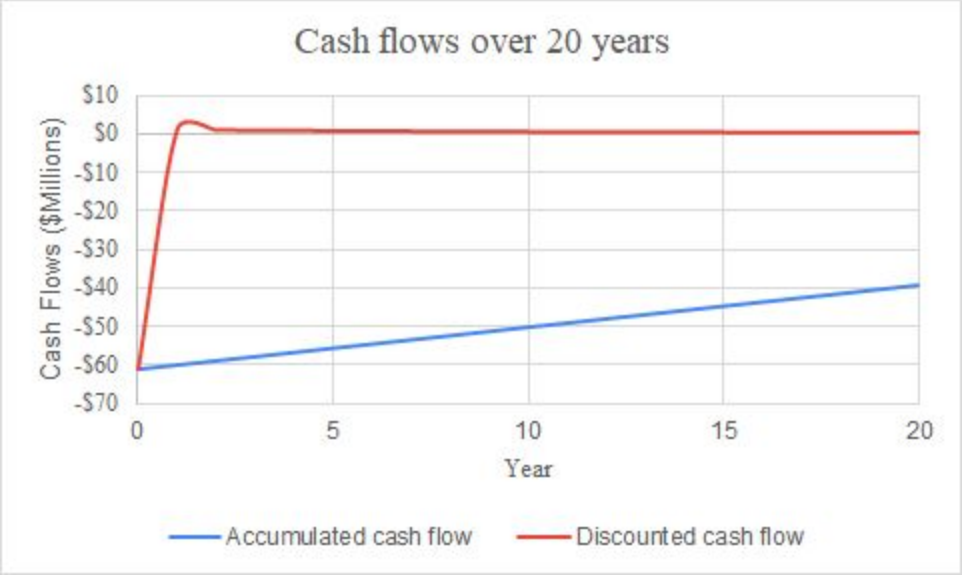

Figure 7.1-3: Projected cash flows over 20 years.

The annual cost of CO_2 storage is $4,479,512, which accounts for 81% of waste treatment costs. This cost is based on a storage cost of $66.5 per tonnes of CO_2, which is the average storage cost for CO_2 storage according to Budinis et al.. The annual wastewater cost, entirely from the carbon capture process, is $77.58. This cost is based on Black & Veatch's 2019 report specifying the average U.S. industrial wastewater cost. Assuming that our process lacks carbon capture and storage, a break-even analysis shows that a break-even occurs after four years (see Figure 7.1-4). When performing the break-even analysis to determine the profitability of our

plant in the absence of carbon capture and storage, we assumed a 50% taxation rate, which is the highest taxation rate according to Turton et al., and a 7% annual discount rate. We determined the IRR to be 40.7% with these assumptions.

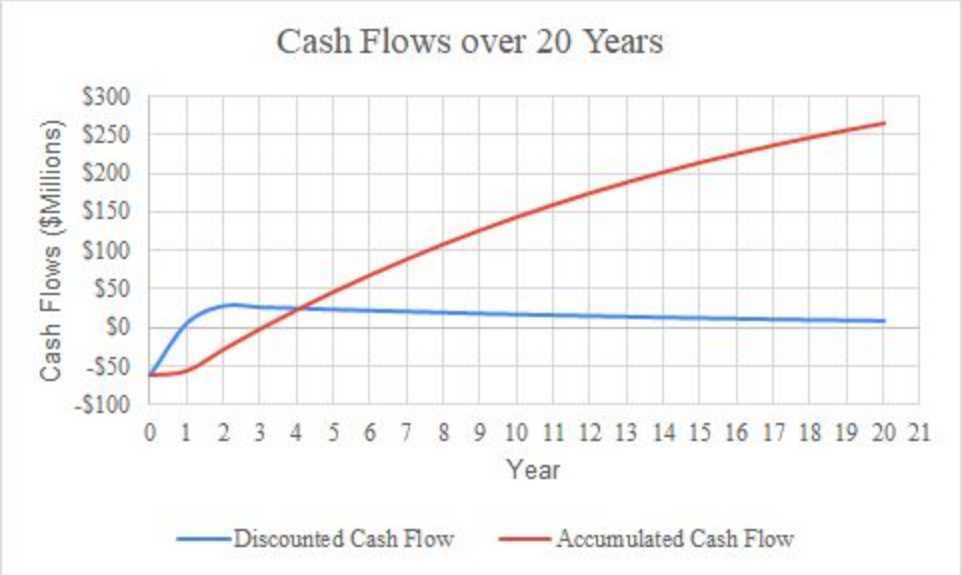

Figure 7.1-4: Projected cash flows assuming a 20-year plant life and no carbon capture and storage. Analysis assumes a 50% taxation rate and a discount rate of 7%.

Although glass and metals recovered from MSW can be usually sold as scrap metal and glass, we are not sure if the glass and metals recovered in our plant will be of sellable quality. We accounted for this uncertainty in our economic analysis to avoid overestimating potential revenue and returns on investment. The total revenue generated annually minus potential revenue from the sale of glass and metals is $13,362,280, which is $17,320,358 less than our annual cost of manufacturing excluding carbon capture and storage, and $22,830,157 with it(carbon capture and storage). A break-even analysis showed that with the total lack of revenue from the sale of metals and glass, a break-even did not occur over a period of 20 years even with the absence of carbon capture and storage (see Figure 7.1-5).

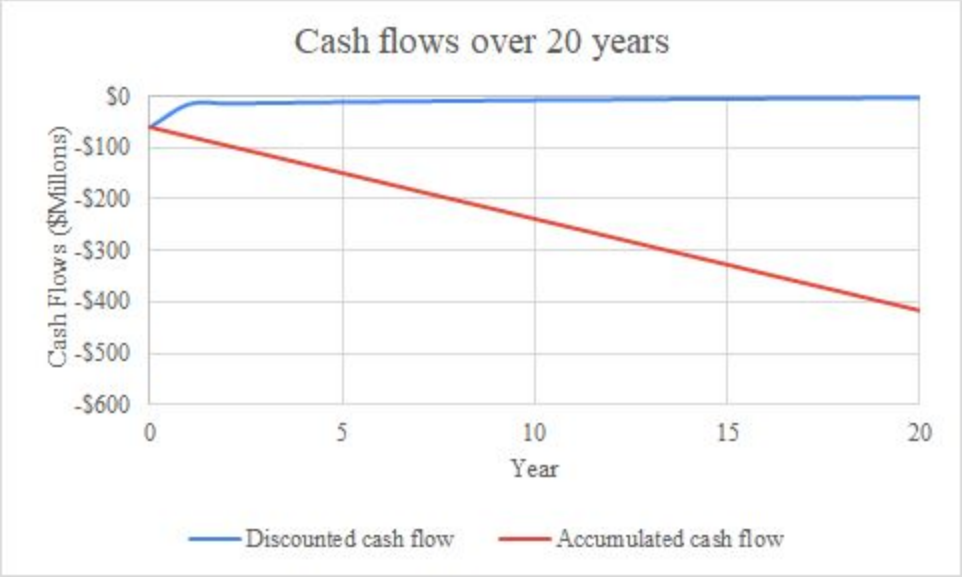

Figure 7.1-5: Projected cash flows assuming no carbon capture and no revenue from sale of recovered metals and glass.

To overcome the lack of profit over the lifetime of the plant, we could sell electricity for a higher price and increase the tipping fee we charge for MSW. A tipping fee greater than $101 per 1000 kilograms of MSW in Boulder, Colorado, is impossible to implement in the area considering that tipping fees typically range from $80-$101 per 1000 kilograms of waste in the region. Furthermore, even tripling the tipping fee has no effect on the break-even analysis because it remains that a break-even does not occur over the life of the plant. Although tipping fees could increase as the city aims to reduce the amount of waste sent to landfill, it is unlikely that tipping fees will double or triple in the region. Electricity prices across the nation have only risen by 15% over the past 10 years (United States Energy Information Administration, 2020). Assuming a similar increase in electricity prices over the next 20 years, our break even analysis remains the same and no profit is projected to be generated over the life of the plant.

8. Conclusions and Recommendations

Considering the economic analysis we carried out on our plant over a lifetime of 20 years, our plant will only generate profits if we vent all the CO_2 to the atmosphere and sell recovered metals and glass at their respective minimum price when sold as scrap, and. As already stated, there is great potential for recovered metals and glass to be sold as scrap material. Venting all the CO_2 produced in our process would add 61 million tons of CO_2 to the atmosphere annually, immensely contributing to a green-house effect and making our process less environmentally friendly. Selling the electricity generated by our plant at a price substantial enough to make our plant profitable over its lifetime is an impossible approach considering estimates of electricity prices in the next 20 years. Similarly, a tipping fee substantial enough to overcome our deficit is impossible to implement in Boulder, Colorado, considering the tipping fee range in the area. Although our analysis only considers that ash will be landfilled, the ash could also potentially be a source of revenue as it is applied in construction activities and as a fertilizer in agricultural activities. In the ideal case where our plant generates revenue from tipping fees, the sale of electricity, and the sale of recovered metals and glass, all in the absence of carbon capture and storage, we estimate an IRR of 40.67% and a NPV of $265,375,362 over a 20-year lifetime. Without revenue from the sale of metals, our plant operates at a deficit of $13,362,280 annually without carbon capture and storage, and $22,830,157 annually with carbon capture and storage.

Our plant is expected to have minimal greenhouse gas emissions as all the carbon dioxide produced in it is captured and stored underground, while methane is used as fuel in the SOFC to generate electricity. Due to this, our plant can be considered environmentally friendly, especially considering that it is converting MSW to a useful and greatly needed product in energy.

Although there are various environmental hazards associated with carbon capture and storage, we anticipate the associated hazards not to be a problem for our plant due to its relatively short lifetime; carbon capture and storage commonly starts to pose environmental problems if intensively carried out over 100 years. However, the feasibility of storing the carbon dioxide captured underground in the city of Boulder, Colorado, remains largely unknown and needs to be researched.

The overall plant efficiency is 25.1% and the efficiency of the SOFC and Rankine cycle systems are 60% and 19% respectively. To improve efficiency, more research is recommended on ways to produce more power. Considering that our operating temperature was based on the optimal ratio of CO to CO_2 in our syngas, more operating temperatures for the gasifier, especially those greater than 700°C, can be explored to maximize the H_2 content in the syngas. Another suggestion is to run multiple Rankine cycles in series, such that the heat waste of one may be used as the heat source for another. This practice would generate significantly more electricity in our case, as the standalone Rankine cycle incorporates approximately 8 MJ/s of lost heat.

9. Acknowledgments

We would like to show gratitude to the individuals who helped us in various aspects of this design project. We would like to acknowledge Professor Eric Anderson of the Chemical Engineering department at the University of Virginia, who served as our team's technical advisor and provided guidance and support throughout the entirety of this design project. We would also like to acknowledge Professor Giorgio Carta of the Chemical Engineering department at the University of Virginia, for his advice in designing heat exchangers.

10. Appendix

Sample Calculation 1: Determining Gasifier Diameter and Height.

$$Hearth\ load\ (\frac{kg}{m^2 h}) = \frac{Mass\ of\ MSW\ gasified\ per\ hour}{Cross\ sectional\ area\ of\ gasifier}$$

Typical hearth load of an updraft gasifier = 150 kg/m^2. hr

MSW feed to the gasifier = 7583 kg/hr = MSW gasified per hour

$$Cross\ sectional\ area\ of\ gasifier\ = \pi r^2$$

Solving for the radius, r, r = 4.1 meters

Using a radius of 2 m to reflect maximum diameter of 4 m and maintaining the hearth load:

$$Mass\ of\ MSW\ gasified\ (\frac{kg}{hr}) = 150\ (kg/m^2 hr) * \pi * 2^2 (m^2)\ = 1,885.7\ kg/hr$$

Mass of MSW gasified per hour = 1,885.7 kg/hr

Using a ratio of height to diameter of 3:1, gasifier height = 4 meters * 3 = 12 meters

Sample Calculation 2: Calculations for Screw Conveyor Moving Ash from Gasifier.

Density of ash = 1,1217.5 kg/m^3 (Amaya et al., 2007)

Flow rate of tars = 1,289 kg/hr

$$Capacity\ (m^3/hr)\ = \frac{Flow\ rate\ (kg/hr)}{Density\ of\ tars\ (kg/m^3)}$$

Capacity (C) = 1.14 m^3/hr

Recommended trough loading = 30% A (obtained from KWS website)

Capacity Factor for cut and folded flights with 30% A trough loading (CF) = 3.75 (obtained from KWS website)

Recommended pitch screws from KWS website: 2/3 pitch screws

Capacity Factor for 2/3 pitch screws (CP) = 1.5 (obtained from KWS website)

Selection capacity (SC) = C *CP* CF = 9.186 m^3/hr

With the calculated SC, screw pitch diameter from KWS website = 2.4 cm

Capacity at 1 RPM = 0.04248 m^3/hr

Auger speed = $\frac{Capacity}{Capacity\ at\ 1\ RPM}$ = 26.8 RPM

Using KWS screw conveyor horsepower guide, power = 0.12 kW

Sample Calculation 3: Determining volume of the syngas cleanup packed bed reactor

The contaminated syngas contains a total of 2,600 kmol of hydrogen sulfide per year

$$ZnO_{(s)} + H_2S_{(g)} \rightarrow ZnS_{(s)} + H_2O_{(g)}$$

For 30% excess zinc oxide, the amount of zinc oxide needed will be equivalent to:

$$2,600\ kmol\ H_2S * \frac{1\ kmol\ ZnO}{1\ kmol\ H_2S} * 1.3 \simeq 3,380\ kmol\ ZnO$$

$$3,380\ kmol\ ZnO * \frac{81.38\ kg\ ZnO}{kmol\ ZnO} \simeq 280,000\ kg\ ZnO$$

Given the density of ZnO ($\rho = 5610$ kg/m^3), the volume of the particles($V_{particles}$) is found by:

$$V_{particles} = 280,000\ kg\ ZnO * \frac{m^3}{5610\ kg} \simeq 49 m^3$$

To determine the size of the vessel, assume a void fraction of 0.39:

$$V_{reactor} = \frac{V_{particles}}{1-\varepsilon} = \frac{0.49\ m^3}{1-0.39} = 80.5\ m^3$$

Sample Calculation 4: Ergun equation and void fraction:

Assume a diameter of the vessel (D_R=3 m) and particles (D_P=0.006) to determine void:

$$\varepsilon = \frac{1.74}{((D_R/D_p)+1.140)^2} + 0.39 = \frac{1.74}{((3/0.006)+1.140)^2} + 0.39 \simeq 0.39$$

To determine the length of the reactor (L), find cross sectional area (A) given diameter of reactor (D_R), then correlate area to volume of reactor:

$$A = \frac{\pi D_R^2}{4} = \frac{\pi\ (3m)^2}{4} = 7.07\ m^2$$

$$V_{reactor} = 80.5m^3 = A * L = 7.07m^2 * L$$

$$L = \frac{80.5m^3}{7.07m^2} = 11.4\ m$$

The superficial viscosity can be found by dividing volumetric flow rate of fluid (Q) by area (A):

$$\nu_s = \frac{Q}{A} = \frac{0.98\ m^3/s}{7.07\ m^2} = 0.14\ m/s$$

Given the density (ρ=0.53kg/m^3) and the viscosity (μ=2.9*10^{-5} Pa*s) of the fluid, solve for change in pressure:

$$\Delta P = \frac{150\mu L}{D_P{}^2}\frac{(1-\varepsilon)^2}{\varepsilon^3}v_s + \frac{1.75L\rho}{D_P}\frac{(1-\varepsilon)}{\varepsilon^3}v_s|v_s|$$

$$= \frac{150(2.9*10^{-5}Pa\ s)(11.4m)}{(0.006\ m)^2}\frac{0.61^2}{0.39^3}(0.14\ m/s) + \frac{1.75(11.4m)(0.53\ kg/m^3)}{0.006\ m}\frac{0.61}{0.39^3}(0.14\ m/s)^2 = 3200\ Pa = 0.015\ bar$$

Sample Calculation 5: Water Gas Shift Calculations

10.4-1 Tube volume can be calculated using the catalyst volume which was found to be 0.76 m^3 and void bed is 0.4 substituting in the equation below tube volume was found to be 1.26 m^3. The area was calculated using the specified diameter of 10 cm and the tube length was determined using the and volume and area of the tube.

$$V_{tube} = V_{cat} + \varepsilon V_{tube} \Rightarrow V_{tube} = 0.76 + 0.4V_{tube}$$

10.4-2 Calculating the area of duty for the reactor

$$Q = AU\Delta T_{LMTD}$$

$$A = \frac{Q}{U\Delta T_{LMTD}}$$

where Q = 490000 Watts, U = 30 W/m^{2}K, ΔT_{LMTD} = 216 K

$$A = \frac{490000}{30*216} \Rightarrow 75\ m^2$$

Sample Calculation 6: Heat Exchanger HX201 Calculation

The area of duty of HX201 can be calculated using the equation used for A_{duty} shown in 10.4-2

Starting with calculating the log mean temperature difference (LMTD) using the following equation, where $T_{hot\ in}$ = 700, $T_{hot\ out}$ = 400, $T_{cold\ in}$ = 184, $T_{cold\ out}$ = 184, Q= 1.26E06 W, U = 30 W/m^{2}k

$$\Delta T_1 = 516,\ \Delta T_2 = 216$$

$$\Delta T_{LMTD} = \frac{\Delta T_1 - \Delta T_2}{ln(\frac{\Delta T_1}{\Delta T_2})}$$

$$= \frac{516-216}{ln(\frac{516}{216})} \Rightarrow 344.5$$

$$A = \frac{1.26*10^6}{30*344.5} \Rightarrow 121.46\ m^2$$

Sample Calculation 7: Fuel Cell Operating Conditions

Utilization Factor (Assumed) = U_f = 0.85
Moles of H_2 Entering Anode = n_{H_2} = 120.8 *kmol/hr*
Moles of CO Entering Anode = n_{CO} = 7.21 *kmol/hr*
Moles of CH_4 Entering Anode = n_{CH_4} = 26.5 *kmol/hr*
Faraday's Constant = F = 96,485 *C/mol*
Temperature = T = 1,000 ^oC
Temperature (Reference) = T = 1,000 ^oC
Pressure = P = 3 *bar*
Pressure (Reference) = P = 1 *bar*
Average Molar Fraction of H_2 = x_{H_2} = 0.173
Average Molar Fraction of H_2O = x_{H_2O} = 0.527
Average Molar Fraction of H_2 (Reference) = x_{H_2} = 0.371
Average Molar Fraction of H_2O (Reference) = x_{H_2O} = 0.411
Average Partial Pressure of O_2 = x_{O_2} = 0.63 *bar*
Average Partial Pressure of O_2 (Reference) = x_{O_2} = 0.21 *bar*
Voltage = V = 0.687 *V*
Current Density = J = 0.185 *A/cm*^{2}
Cell Active Area = A_{cell} = 834 *cm*^{2}
Cells per Stacks = n_{cell} = 1152
Number of Stacks = n_{stack}
Power = P
Voltage (Reference) = V_{ref}

From the reactive equations (5-7) and the utilization factor, the amount of O_2 that reacts electrolytically and diffuses across the barrier may be computed:

$$n_{O_2(Diffused)} = U_f \cdot \left(n_{H_2} + n_{CO} + 4n_{CH4} \right) = 98.9 \; kmol/hr$$

The equivalency in total current is then computed based on this rate of diffusion. Note that the coefficient comes from the electron stoichiometry:

$$I = 4F \left(n_{O_2(Diffused)}[mol/s] \right) = 10.6 \cdot 10^6 \; Amps$$

To determine the power, the voltage must be found by consulting voltage curves in the DoE Fuel Cell Handbook. Curves are provided at a set of reference conditions and shifted from this reference via correlations. Note that the averages are taken from inlet and outlet values, since gradients are unknown.

$$\Delta V_{anode} = 172 log \left(\frac{P_{H_2}/P_{H_2O}}{\left(P_{H_2}/P_{H_2O}\right)_{ref}} \right) = 172 log \left(\frac{x_{H_2}/x_{H_2O}}{\left(x_{H_2}/x_{H_2O}\right)|_{ref}} \right) = \; -0.076 \; V$$

$$\Delta V_{cathode} = 92 log \left(\frac{P_{O_2}}{P_{O_2}|_{ref}} \right) = 0.050 \; V$$

$$\Delta V_{temp.} = f(T - T_{ref}) = 0$$

$$\Delta V_{pressure} = 59 log \left(\frac{P}{P|_{ref}} \right) = 0.033 \; V$$

The updated voltage at any point along the curve is a summation. Since the net contribution of the adjustment terms is negligible, the updated voltage is assumed as the reference.

$$V = V_{ref} + \Delta V_{anode} + \Delta V_{cathode} + \Delta V_{temp.} + \Delta V_{pressure} \simeq V_{ref}$$

The true power output per stack is assumed as that in Zhang's model (120 kW). A goalseek method was employed for this purpose, as illustrated for the correct voltage and its

corresponding current density. Total power across the stacks was first determined, followed by the number of stacks.

$$P = IV = 7.29 \cdot 10^6\ W$$

$$n_{stack} = I/(J \cdot n_{cell} \cdot A_{cell}) = 60\ stacks$$

$$\therefore P/n_{stacks} = 121.5\ kW \simeq 120\ kW\ (solution\ is\ correct)$$

Sample Calculation 8: Optimizing Rankine Cycle

Power = P $[J/s]$
Exhaust Molar Flow Rate = $n_{exh.}$ $[kmol/hr]$
Exhaust Heat Capacity = $C_{P(exh.)}$ $[J/kmol\ K]$
Exhaust Inlet Temperature = $T_{in(exh.)} = 1462K$
Steam Inlet Temperature = $T_{water(cold)} = 298K$
Steam Outlet Temperature = $T_{water(hot)} = 639K$

An energy balance is made around HX-302 assuming that all enthalpic changes in the exhaust are the source of power. The Carnot efficiency term accounts for ideal heat losses, yet the model assumes negligible heat and frictional losses throughout the piping. The water's and exhaust's outlets are assumed to converge upon the same temperature: $T_{water(hot)}$ …

$$P = n_{exh.} C_{P(exh.)} \left(T_{in(exh.)} - T_{water(hot)}\right)\left(1 - T_{water(cold)}/T_{water(hot)}\right)$$

Taking the derivative with respect to $T_{water(hot)}$ and setting equal to zero gives the optimum outlet temperature.

$$\therefore T_{water(hot)}|_{max\ power} = \sqrt{T_{in(exh.)} T_{water(cold)}} = 387^o C$$

As discussed, this temperature is in the supercritical regime, and therefore a temperature was chosen as close as reasonably possible to the critical point.

Sample Calculation 9: Estimating Operating Labor Costs

According to *Analysis, Synthesis, and Design of Chemical Processes, Fourth Edition,* the number of operators per shift, N_{OL}, is estimated as:

$$N_{OL} = (6.29 + 31.7P^2 + 0.23N_{np})^{0.5}$$

where P is the number of processing steps involving handling of particulate solids, N_{np} is the number of nonparticulate processing steps and includes compression, heating and cooling, mixing, and reaction.

Equipment Type	Number of Equipment	N_{np}
Compressors	1	1
Exchangers	9	9
Heaters/Furnaces	6	6
Reactors	5	10
Towers	0	0
Vessels	4	4
Total		25

To account for the four processing steps that occur during feedstock preparation, namely: recovery of metals, shredding, removal of glass, and transportation of MSW from storage, P was set to 4.

Substituting for P and N_{np} to calculate N_{OL}:

$$N_{OL} = (6.29 + 31.7 * 4^2 + 0.23 * 25)^{0.5} = 22.79 \text{ operators} = 23 \text{ operators}$$

According to *Analysis, Synthesis, and Design of Chemical Processes, Fourth Edition,* 4.5 operators are hired for each operator needed in the plant at any time.

$$\textit{Operating Labor} = 4.5 * 23 = 104 \textit{ operators}$$

Annual salary of a plant operator in Boulder, Colorado is $30,000 (Glassdoor)

Annual operating labor costs (C_{OL}) = $104 * 30,000$ = $3,829,195.9

Sample Calculation 10: carbon capture separators' area and diameter

The separator area was calculated using equation 5.7-1 and the vapor volumetric flow rate

$u_{Perm} = K_{drum}\sqrt{\frac{\rho_v - \rho_L}{\rho_v}}$ where $K_{drum} = 0.35$, $\rho_v = 0.14$ lb/ ft , $\rho_L = 61.6$ Ib/ft, $Q_v = 139.75$

$u_{perm} = 0.35 * \sqrt{\frac{0.14-61.6}{0.14}} \Rightarrow 2.75\, ft/s$

$A = \frac{Q_V}{u_{perm}} = \frac{139.75}{2.75} = 50.84\, ft^2 \Rightarrow 4.72\, m^2$

$A = \pi r^2 \Rightarrow r = 1.2\, m,\ D = 2.45\, m$

Sample Calculation 11: After-Tax Net Income, and After-Tax ROI

According to *Analysis, Synthesis, and Design of Chemical Processes, Fourth Edition,* cost of manufacturing (COM) can be calculated from

$COM = 0.280\, FCI + 2.37 C_{OL} + 1.23\, (C_{UT} + C_{RM} + C_{WT})$

Where:

COM is cost of manufacturing

FCI (fixed capital investment or total plant capital costs) = $54,129,779

C_{OL} (cost of of operating labor annually) = $3,076,223.2

C_{UT} (cost of utilities annually) = $8,733,883

C_{RM} (cost of raw materials annually) = $0 because we are paid to handle MSW, which is our raw material and accounted for as a source of revenue

C_{WT} (cost of waste treatment annually) = $1,996,460 (disregarding costs of carbon capture and storage).

$$COM = 0.280\ (\$54,129,779) + 2.37(3,076,223.2) + 1.23\ (\$8,733,833 + \$\$1,996,460 + \$0) = \$30,682,638$$

$$Annual\ revenue\ (see\ section\ 5) = \$31,664,680$$

According to *Analysis, Synthesis, and Design of Chemical Processes, Fourth Edition*, overall taxation rates range from 40% to 50%. We only tax gross profits (for revenue-cost of manufacturing>0).Assuming a 50% taxation rate:

$$After-tax\ profit = (Revenue - COM) * tax\ rate$$

$$After-tax\ profit = (\$\$31,664,680 - \$30,682,638) * 50$$

$$After-tax\ profit = \$491,021$$

$$After-tax\ ROI = \frac{After-tax\ profit}{Total\ plant\ capital\ cost} * 100\% = \frac{\$\$491,021}{\$\$66,355,747} * 100\% = 0.74\%$$

Sample Calculation 12: Determining Steam Production in a Heat Exchanger

Given that the heat duty (Q) of the heat exchanger is equal to 1,260,000 J/s and the cooling water inlet temperature is 184°C, we can determine the steam produced using the heat of vaporization, ΔH_{vap}.

According to The Engineering Toolbox, at 184°C, ΔH_{vap} = 1999.8 kJ/kg

To determine mass flow rate (m) of steam,

$$m = \frac{Q}{\Delta H_{vap}} = \frac{1{,}260{,}000\ J/s}{(1999.8\ kJ/kg)(1000\ J/kJ)} = 0.63\ kg/s$$

Sample Calculation 13: Determining Cooling Water Flow Requirement in Heat Exchanger

Given that the heat duty (Q) of the heat exchanger is equal to 556,000 J/s and the cooling water change in temperature (ΔT) is 10 K, the mass flow rate (m) of the fluid is found using:

$$Q = mC_P\Delta T$$

According to the Engineering Toolbox, C_P = 4180 J/(kg*K) for water at 25C

$$m = \frac{Q}{C_P\Delta T} = \frac{556{,}000\ J/s}{(4180\ J/kg*K)(10\ K)} = 13.3\ kg/s$$

Sample Calculation 14: Overall Plant Efficiency

Efficiency for the overall plant was calculated using the following equation:

$$\%\ Efficiency\ = 100 * \frac{Net\ Power\ Generation}{Energy\ Contained\ in\ Waste}$$

$$Energy\ Contained\ in\ Waste\ =\ LHV_{waste} * mass_{waste}$$

$$Energy\ Contained\ in\ Waste\ =\ (13,460\ kJ/kg) * (205,656\ kg/day)(\frac{day}{24\ hr})(\frac{hr}{3600\ s}) = 32.46\ MW$$

The LHV of the MSW is assumed to be approximately 13640 kJ/kg based on 2005 data from the Energy Information Administration. The net power generation was 7.82 MW after factoring in power integration.

$$\%\ Efficiency\ = 100 * \frac{Net\ Power\ Generation}{Energy\ Contained\ in\ Waste} = \frac{7.82\ MW}{32.46\ MW} = 24.1\%$$

Sample Calculation 15: Solid Oxide Fuel Cell and Rankine Cycle Efficiencies

The power output of the fuel cell was determined through *sample calculation 7* for reference. The ASPEN model of the fuel cell reports heat duty as the sum of the power and heat losses of an isothermal cell, assuming all inlets and outlets are provided at operating temperature.

$$\%Efficiency = \frac{P}{P+Q_{loss}} \cdot 100\% = (7.29\ MW)/(7.29\ MW + 4.86\ MW) \cdot 100\% = 60\%$$

The heat inlets and outlets from the Rankine Cycle are also provided in the ASPEN model. A net power is defined that deducts the power demands of the cycle's compressor from the turbine.

$$\%Efficiency = (P_{turbine} + P_{compressor})/H_{in} = (2.193\ MW - 0.178\ MW)/11.5\ MW = 19.1\%$$

11. References

Adams II, Thomas A. and Barton, Paul I. (2009). *A dynamic two-dimensional heterogeneous model for water gas shift reactors*. International Journal of Hydrogen Energy 34, 8877–8891.

Ali Liquide. (2018) Carbon monoxide. *Safety Data Sheet*. Retrieved from: http://alsafetydatasheets.com/download/no/Carbon_monoxide_NOAL_0019_NO_EN.pdf

Amaya, J., P., Amaya, J., A. (2007,May 7). The use of bottom ash in the design of dams. Retrieved from: http://www.flyash.info/2007/66amaya.pdf

Barnard, M. (2016, January 19). Carbon capture is expensive because physics. *CleanTechnica.* Retrieved from: https://cleantechnica.com/2016/01/19/carbon-capture-expensive-physics/

BASF. (2002). Catalyst Data Sheet - ZnO for H2S Removal. Retrieved from: http://www.psbindustries.com/pdf/BASF%20R5-12%20Data%20Sheet.pdf

Basu. P. (2010). *Biomass Gasification and Pyrolysis: Practical Design*. Burlington, MA: Elsevier Inc.

Begum, S., Rasul, M.G., Akbar, D., Ramzan, N. (20*14). A Numerical Investigation of Municipal Solid Waste Gasification Using Aspen Plus. Procedia Engineering, Vol 90, pages 710-717,* doi:10.1016/j.proeng21411800

Bhada-Tata, P., & Hoonrweg, D. (2012, March). What a waste: a global review of solid waste management. *Urban Development Series – Knowledge Papers*, *15*. Retrieved from https://siteresources.worldbank.org/INTURBANDEVELOPMENT/Resources/336387-1334852610766/What_a_Waste2012_Final.pdf

Black & Veatch. (2019). 50 Largest cities water and wastewater survey. *Black & Veatch Management Consulting, LLC.* Retrieved from: https://www.bv.com/sites/default/files/2019-10/50_Largest_Cities_Rate_Survey_2018_2019_Report.pdf

Boulder County. (2005). Boulder county zero waste action plan. Retrieved from: https://www.colorado.edu/ecenter/sites/default/files/attached-files/5_boulder_zerowasteactionplan.pdf

Budinis, S., Krevor, S., Dowell, N.M., Brandon, N., Hawkes, A. (2018, November). An assessment of CCS costs, barriers, and potential. *Energy Strategy Reviews, 22,* 61-81. doi:10.1016/j.esr.2018.08.003

Bulk Apothecary. (n.d.) Zinc Oxide. https://www.bulkapothecary.com/product/raw-ingredients/other-ingredients-and-chemicals/zinc-oxide/

City of Boulder. (2020). We are zero waste Boulder. Retrieved from: https://bouldercolorado.gov/zero-waste

Davis, M.E., Davis, R.J. (2013). *Fundamentals of Chemical Reaction Engineering.* Newburyport: Dover Publications.

Economic indicators. 2020. *Chemical Engineering* 127, (2) (02): 56, http://proxy01.its.virginia.edu/login?url=https://search.proquest.com/docview/2354854738?accountid=14678 (accessed March 25, 2020).

EG&G Technical Services. (2004, November). *Fuel Cell Handbook*. (7th ed.). https://www.netl.doe.gov/sites/default/files/netl-file/FCHandbook7.pdf

Energy Information Administration. (2007, May). Methodology for Allocating Municipal Solid Waste to Biogenic and Non-Biogenic Energy. https://www.eia.gov/totalenergy/data/monthly/pdf/historical/msw.pdf

EPA (n.d.). *Waste Transfer Stations: A manual for decision-making*. https://www.epa.gov/sites/production/files/2016-03/documents/r02002.pdf

Funk, K., Milford, J., & Simpkins, T. (2013, February). Waste not, want not: analyzing the economic and environmental viability of waste-to-energy (WTE) technology for site-specific optimization of renewable energy options. https://www.nrel.gov/docs/fy13osti/52829.pdf

Federal Highway Administration (n.d.). Retrieved from https://www.fhwa.dot.gov/publications/research/infrastructure/pavements/97148/033.cfm

Felder, M. R. and Rousseau, R. W. (2005). *Elementary Principles of Chemical Engineering* (3rd ed.). Wiley.

Ferrara, G., Lanzini, A., Leone, P., Ho, M.T., Wiley, D.E. (2017). Exergetic and exergoeconomic analysis of post-combustion CO2 capture using MEA-solvent chemical absorption. *Energy, 130,* 113-128. doi:10.1016/j.energy.2017.04.096

Golam, R. (2016, July). Characterization and assessment of the potential of local biomass as feedstock of synthetic fuels and chemicals. Retrieved from: https://pdfs.semanticscholar.org/71af/bf315dbc23322da1432b6a89ed01ee84b0d0.pdf

Gupta, R. (2007, August). High-temperature sulfur removal in gasification applications. *Center for Energy Technology RTI International.* Retrieved from: https://www.topsoe.com/sites/default/files/gupta.pdf

Joseph, A., Ruben, S., Snellings, R., Heede, P., Matthys, S., & Belie, N. (2018, January, 11). The use of municipal solid waste incineration ash in various building materials: a belgian point of view. *United States National Library of Medicine-National Institute of Health*. Retireved from https://www.ncbi.nlm.nih.gov/pmc/articles/PMC5793639/

Klein, A. (2002, May). *Gasification: An Alternative Process for Energy Recovery and Disposal of Municipal Solid Wastes*. http://www.seas.columbia.edu/earth/kleinthesis.pdf

KWS (n.d.). Screw Conveyor Capacity. https://www.kwsmfg.com/engineering-guides/screw-conveyor/screw-conveyor-capacity

Lima, D., Zanella, F., Lenzi, M., & Ndiaye, P. (2012, March). Modeling and simulation of water gas shift reactor: an industrial case. doi: 10.5772/37181

Lopamudra, R., Tapan, K.A. (2020). *Energy, nutrient, and water resource recovery from agriculture and aquaculture wastes.* Retrieved from: https://www.sciencedirect.com/science/article/pii/B9780444643216000185?via%3Dihub

Luis, P. (2016). Use of monoethanolamine (MEA) for CO2 capture in a global scenario: consequences and alternatives. *Desalination, 380,* 93-99. doi:10.1016/j.desal.2015.08.004

Marcantonio, V., Bocci, E., Ouweltjes, J.P., Zotto, L.D., & Monarca, D. (2020). Evaluation of sorbents for high temperature removal of tars, hydrogen sulphide, hydrogen chloride, and ammonia from biomass-derived syngas by using Aspen Plus. *International Journal of Hydrogen Energy, 45*(11), 6651-6662. doi:10.1016/j.ijhydene.2019.12.142

MEA Safety Datasheet (2009, June, 11.). Retrieved from https://www.fishersci.com/store/msds?partNumber=M2514&productDescription=ETHANOLAMINE+PURIFIED+4L&vendorId=VN00033897&countryCode=US&language=en

Metal Prices (n.d.). https://www.priceofscrapmetals.com/colorado/

Midilli, A., Dogru, M., Howarth, C., Ling, M., Ayhan, T. (2001, January). Combustible gas production from sewage sludge with a downdraft gasifier. *Energy of Conversion and Management. 42*(2). 157 -172. doi: 10.1016/S0196-8904(00)00053-4

Molino, A., Chianese, S., Musmarra, D. (2016). Biomass gasification technology technology: The state of the art overview. *Journal of Energy Chemistry*, 25(1),10-25. doi;10.1016/j.jechem.2015.11.005

Monterey Park (n.d.). *Materials Recovery Facility*. Retreived from https://www.montereypark.ca.gov/554/Materials-Recovery-Facility

Newsome, David S. (1980). The water-gas shift reaction. Catal. Rev. Sci. Eng., 21(2), 275-318. Singh, C. C. P. and Saraf, D. N. (1977). Simulation of high-temperature water-gas shift Reactors. Ind. Eng. Chem. Process Des. Dev., Vol. 16, No. 3, 313-319.

NIOSH (2004, August.). Methane Safety. Retrieved from https://www1.agric.gov.ab.ca/$department/deptdocs.nsf/all/agdex9038/$file/729-2.pdf?OpenElement&fbclid=IwAR1kqzolBzj46xk1fyTuQULkl3dsQiYdDI8LlIcnVLbVhEPQ33HIycI7v_c

O'Neill, K. (2018, December 4). The plastic waste crisis is an opportunity for the U.S. to get serious about recycling at home. *The Conversation*. Retrieved from https://theconversation.com/the-plastic-waste-crisis-is-an-opportunity-for-the-us-to-get-serious-about-recycling-at-home-93254

OSHA (n.d.). *Carbon monoxide Poisoning*. https://www.osha.gov/OshDoc/data_General_Facts/carbonmonoxide-factsheet.pdf

Peters, M.S., Timmerhaus, K.D., West, R.E. (2006) *Plant design and economics for chemical engineers* (5th ed.). Boston: McGraw-Hill.

Petrovic, B.A. & Soltani, S.M. (2019). Optimization of post combustion CO2 capture from a combined-cycle gas turbine power plant via taguchi design of experiment. *Processes, 7(*6), 364. doi:10.3390/pr7060364

PumpScout Staff. (2019). “Pump Types Guide - Finding the Right Pump.” PumpScout. http://www.pumpscout.com/articles-scout-guide/pump-types-guide-aid100.html

Ralston, A. (2004). *Between a Rock and a Hard Place*. ISBN-13: 1-4165-0510-5

Recycling Product News (2017, December, 07). https://docs.google.com/document/d/1VIZVCOwbjIzcR2biUbHNd0Lj9hOji_UdILb5wRwIZCo/edit#

Rasul, G. (2016). Characterization and assessment of the potential of local biomass as feedstock of synthetic fuels and chemicals. Retrieved from https://pdfs.semanticscholar.org/71af/bf315dbc23322da1432b6a89ed01ee84b0d0.pdf

Sadegh-Vaziri, R., Babler, M.U. (2019). Removal of hydrogen sulfide with metal oxides in packed bed reactors--a review from a modeling perspective with practical implications. *Applied Sciences, 9*(24). doi:10.3390/app9245316

Seader, J., Henley, E., & Roper, D.(2011). Flooding, column diameter, pressure drop, and mass transfer for trayed columns. Separation Process Principles: Chemical and Biochemical Operations.(3rd ed.). 227-232. ISBN 978-0-470-48183-7.

Speight, J. 2016. Production of syngas, synfuel, bio-oils, and biogas from coal, biomass, and opportunity fuels. *Fuel Flexible Energy Generation.* 145-174. doi:10.1016/B978-1-78242-378-2.00006-7

Taufiq, T. (2010). *Characteristics of Fresh Municipal Solid Waste.* https://rc.library.uta.edu/uta-ir/bitstream/handle/10106/4880/Taufiq_uta_2502M_10596.pdf?sequence=1&isAllowed=yF

The Engineering ToolBox. (n.d). https://www.engineeringtoolbox.com/boiling-point-water-d_926.html

Turton, R., Bailie, R. C., Whiting, W. B., Shaeiwitz, J. A., & Bhattacharyya, D. (2016). Analysis, synthesis, and design of chemical processes. UP, India: Pearson India Education Services.

Yong, C.S., Tanvir, A., Won-Seok Y. (2017, June, 11). *Gasification of Municipal Solid Waste, Gasification for Low-grade Feedstock*. DOI: 10.5772/intechopen.73685. Retrieved from: https://www.intechopen.com/books/gasification-for-low-grade-feedstock/gasification-of-municipal-solid-waste

U.S. Department of Energy. (2019, August). Waste-to-energy from municipal solid waste. *Office of Energy Efficiency and Renewable Energy.* https://www.energy.gov/sites/prod/files/2019/08/f66/BETO--Waste-to-Energy-Report-August--2019.pdf

U.S. Energy Information Administration. (2020, March 19). Electricity Explained. https://www.eia.gov/energyexplained/electricity/prices-and-factors-affecting-prices.php

U.S. Environmental Protection Agency (n.d.). Waste transfer stations: a manual for decision-making. Retrieved from: https://www.epa.gov/sites/production/files/2016-03/documents/r02002.pdf

Vinca, A., Emmerling, J., & Tavoni, M.(2018, May). Bearing the cost of stored carbon leakage. *Sustainable Energy Systems and Policies*. Retrieved from: https://doi.org/10.3389/fenrg.2018.00040

Wankat, P .(2016, August). Separation process engineering: includes mass transfer analysis, fourth edition. ISBN: 9780133443714

Warudkar, S.S., Cox, K.R., Wong, M.S., Hirasaki, G.J. (2013). Influence of stripper operating parameters on the performance of amine absorption systems for post-combustion carbon capture: Part II. Vacuum strippers. *International Journal of Greenhouse Gas Control.* doi:10.1016/j.ijggc.2013.01.049

Zhang, W. (2006). Simulation of Solid-Oxide Fuel Cell-Based Power Generation Processes with CO_2 Capture. https://uwspace.uwaterloo.ca/bitstream/handle/10012/946/w23zhang2006.pdf?sequence=1&isAllowed=y